GeoStorage

Vol. 1, No. 2, p. 91-112, 2025

Review article

Recent Progress in CO_2 Mineralization to Mitigate CO_2 Emissions: A Review

Yue Yin[1,2], Liwei Zhang[1,2*], Hanwen Wang[1,2], Manguang Gan[1,2], Yan Wang[1,2], Tianyu Liu[1,2]

[1] *Key Laboratory of Geomechanics and Geotechnical Engineering Safety, Institute of Rock and Soil Mechanics, Chinese Academy of Sciences, Wuhan 430071, China*

[2] *University of Chinese Academy of Sciences, Beijing 100049, China*

Keywords:

Mineralization
CO_2
CGUS
aluminosilicates
basalt
industrial wastes

Cited as:

Yin Y, Zhang LW, Wang HW, et al. 2025. Recent Progress in CO_2 Mineralization to Mitigate CO_2 Emissions: A Review. *GeoStorage*, 1(2), 91-112.
https://doi.org/10.46690/gs.2025.02.01

Abstract:

Global climate warming poses a significant threat to the human living environment, and CO_2 geological utilization and storage (CGUS) technology is regarded as a promising strategy for reducing carbon emissions. CO_2 mineralization represents a crucial aspect of CCUS technologies, offering a safe and stable method for carbon sequestration. Nonetheless, the complex interactions among CO_2, fluids, and minerals present challenges for large-scale mineralization storage. Controlling the carbonation rate under varying reaction conditions proves to be a difficult task. Additionally, carbon mineralization reactions may lead to structural alterations in geological formations and wellbores, which introduces potential risks to the safety of carbon storage. This paper offers a comprehensive review and introduction to the latest advancements of CO_2 mineralization in three scenarios: in oil reservoirs and saline aquifers, in basalt, and through the utilization of solid waste. Following the presentation of representative studies conducted in recent years for each scenario of CO_2 mineralization, this paper discusses the primary challenges exist in the pursuit of greenhouse gas reduction through large-scale CO_2 mineralization. Finally, this review proposes future development directions and strategies to address these challenges. This review serves as a directional reference for future research on CO_2 mineralization.

1 Introduction

The rising concentration of atmospheric carbon dioxide (CO_2) resulting from fossil fuel combustion, deforestation, and industrial processes has been identified as the primary driver of global climate change (IPCC, 2022). To limit global warming to 1.5–2°C above pre-industrial levels, as outlined in the Paris Agreement, aggressive CO_2 mitigation strategies are essential. Among these strategies, CO_2 geological utilization and storage (CGUS) has emerged as a critical technology for reducing anthropogenic CO_2 emissions (Kammerer et al., 2023; Oelkers and Cole, 2008; Zhang et al., 2020). The IPCC has recognized CGUS as a technically feasible approach for achieving significant reductions in CO_2 emissions from the combustion of fossil fuels, the production of fossil fuels, the burning of biomass-based fuels, and certain industrial processes (Tayari and Blumsack, 2020; Xu et al., 2004; Zhang et al., 2009). Typical CGUS methods involve capturing CO_2 from point sources and storing it in deep geological formations, such as oil and gas reservoirs or saline aquifers, as illustrated in Fig. 1.

CO_2 mineralization, commonly referred to as mineral trapping, is one of the key mechanisms that facilitate long-term safe storage of injected CO_2 (Edouard et al., 2023). This process, also known as in-situ mineral carbonation, involves the reaction of CO_2 with reactive minerals in geological formations, thereby converting CO_2 into stable carbonates. This method offers a secure and permanent storage solution (Kumar and Shrivastava, 2019). Through CO_2 mineralization, CO_2 is chemically bound into solid carbonates (e.g., magnesite, calcite), effectively eliminating the risk of CO_2 leakage (Cao et al., 2023).

CO_2 mineralization has three typical scenarios. The first scenario is CO_2 mineralization by aluminosilicates (i.e.,

Yandy Scientific Press

* Corresponding author.
E-mail address: yy_cve@163.com (Yin Y); lwzhang@whrsm.ac.cn (Zhang LW); churchwang@163.com (Wang HW); mggan@whrsm.ac.cn (Gan MG); ywang@whrsm.ac.cn (Wang Yan); 799829767@qq.com (Liu TY)

Received Jul. 18, 2025; revised Aug. 28, 2025; accepted Sep. 5, 2025; available online Sep. 29, 2025.

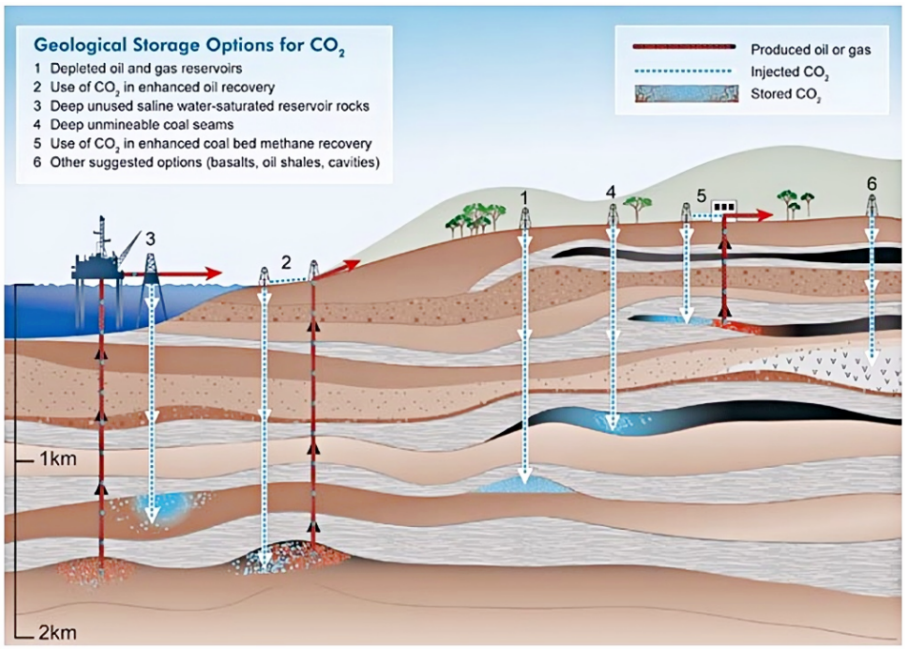

Fig. 1 Demonstration of CGUS (IPCC, 2023)

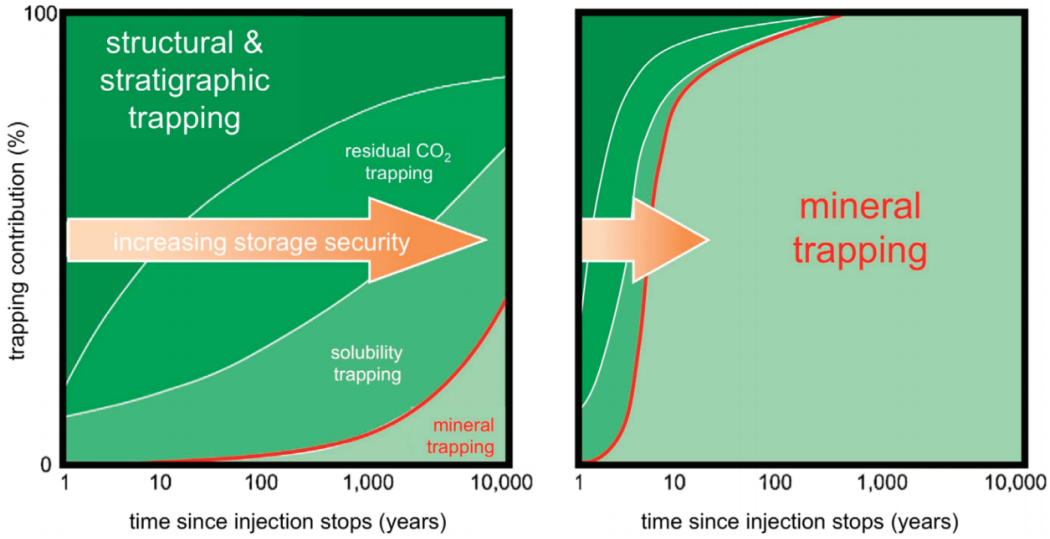

Fig. 2 Comparison between the contribution of mineral trapping in normal sandstone and the contribution of mineral trapping in basaltic and ultramafic rocks (Rani et al., 2013)

$NaAlSiO_3$, $CaAlSiO_3$, etc.), which commonly occurs in sandstone-type oil/gas reservoirs and saline aquifers. The rate of CO_2 mineralization by most aluminosilicates is relatively slow, which only contributes to 10–15% overall CO_2 trapping after 1000 years of CO_2 injection (Dessert et al., 2003; Kump et al., 2000; Moosdorf et al., 2014). Therefore, for most oil/gas reservoirs and saline aquifers, CO_2 mineralization is not regarded as a primary trapping mechanism (Snæbjörnsdóttir et al., 2020). The second scenario is CO_2 mineralization by basaltic and ultramafic rocks. Olivine, serpentines and pyroxenes are the primary contributors to CO_2 mineralization by basaltic and ultramafic rocks. The rate of CO_2 mineralization by olivine, serpentines and pyroxenes is fast, which can contribute to 80% CO_2 trapping only after 10 years of CO_2 injection (Fig. 2). Therefore, CO_2 mineralization in basaltic and ultramafic rocks has garnered significant attention in recent years, emerging as one of the most prominent research areas in CGUS (Lei et al., 2021; Rosenbauer et al., 2012; Wang et al., 2023). The third scenario is CO_2 mineralization by solid wastes exhibiting high reactivity with CO_2, such as high-calcium fly ash, mine tailings, carbide slag, etc. to form solid materials with good mechanical strength (Schaef et al., 2011; Xiong et al., 2017). These materials can be used for backfilling coal mine goafs and other open underground spaces. The CO_2 mineralization approach using solid wastes has attracted widespread attention in recent years, as it not only effectively sequesters CO_2 but also enables the reuse of solid waste materials (Yin et al., 2024). Also, the reaction rate between CO_2 and solid waste materials

is generally fast, so a considerable CO_2 uptake by solid waste materials within a short time frame can be ensured (Oelkers et al., 2019; White et al., 2020).

This review begins by introducing the reaction mechanisms underlying CO_2 mineralization. It then systematically summarizes representative studies conducted in recent years on the aforementioned three scenarios of CO_2 mineralization. Following this, the review addresses the key challenges currently impeding large-scale CO_2 mineralization. Finally, it proposes future research directions and potential strategies to overcome these challenges.

2 Reaction mechanisms of CO_2 mineralization

CO_2 mineralization relies on the chemical reaction between dissolved CO_2 and reactive minerals containing calcium (Ca), magnesium (Mg), iron (Fe), etc. to form stable carbonate minerals. The generalized reaction of CO_2 mineralization can be summarized as Eq. (1):

$$\begin{aligned}&(\mathrm{Mg, Ca, Fe})_x\mathrm{Al}_w\mathrm{Si}_y\mathrm{O}_{3x}(\mathrm{s}) + y\mathrm{CO_2(aq)} \rightarrow \\ &x(\mathrm{Mg, Ca, Fe})\mathrm{CO_3(s)} + w\mathrm{Al^{3+}(aq)} + y\mathrm{SiO_2(aq)}\end{aligned} \quad (1)$$

where, $(\mathrm{Mg, Ca, Fe})_x\mathrm{Al}_w\mathrm{Si}_y\mathrm{O}_z$ represents a general form of minerals containing Ca, Mg and Fe, CO_2 represents dissolved carbon dioxide, $(\mathrm{Mg, Ca, Fe})CO_3$ represents solid carbonates (the stable form in which CO_2 is sequestered), Al^{3+} represents dissolved aluminum ion, SiO_2 represents dissolved silica. Note that Al^{3+}(l) can combine with SiO_2(l) to form clay minerals, and SiO_2(l) can precipitate to form amorphous SiO_2(s) or quartz (Xiong et al., 2017).

The process of CO_2 mineralization typically occurs in three main stages:

(1) Dissolution of CO_2: CO_2 dissolves in formation water, forming carbonic acid (H_2CO_3), which dissociates into bicarbonate (HCO_3^-) and protons (H^+), as shown in Eq. (2).

$$\mathrm{CO_2 + H_2O \leftrightarrow H_2CO_3 \leftrightarrow HCO_3^- + H^+} \quad (2)$$

(2) Mineral dissolution: Protons react with silicate minerals, releasing divalent cations (Mg^{2+}, Ca^{2+}, Fe^{2+}), as shown in Eq. (3).

$$\begin{aligned}&(\mathrm{Ca, Mg, Fe})_2\mathrm{SiO_4} + 4\mathrm{H^+} \rightarrow \\ &2(\mathrm{Ca, Mg, Fe})^{2+} + 2\mathrm{H_2O} + \mathrm{SiO_2}\end{aligned} \quad (3)$$

(3) Carbonate precipitation: Cations react with bicarbonates to form solid carbonates (e.g., magnesite, calcite, siderite), as shown in Eq. (4).

$$(\mathrm{Ca, Mg, Fe})^{2+} + \mathrm{HCO_3^-} \rightarrow (\mathrm{Ca, Mg, Fe})\mathrm{CO_3}\downarrow + \mathrm{H^+} \quad (4)$$

The above reaction process can be illustrated by Fig. 3.

Some representative CO_2 mineralization reactions are summarized below:

(1) Reactions between CO_2 and aluminosilicates in the subsurface, as shown in Eqs. (5)–(7):

Ca-feldspar:

$$\mathrm{CaAl_2Si_2O_8 + 3H_2O + CO_2 \rightarrow CaCO_3 + 2Al(OH)_3 + 2SiO_2} \quad (5)$$

Fe-bearing muscovite:

$$\begin{aligned}&\mathrm{K_4(Fe_{0.5}Mg_{0.5})Al_2Si_3O_{11}(OH)_2 + 4H_2O + 5CO_2} \rightarrow \\ &\mathrm{0.5MgCO_3 + 0.5FeCO_3 + 2Al(OH)_3 + 4K^+ + 3SiO_2 + 4HCO_3^-}\end{aligned} \quad (6)$$

Chlorite:

$$\begin{aligned}&\mathrm{Mg_5Al_2Si_3O_{10}(OH)_8 + 5CO_2} \rightarrow \\ &\mathrm{5MgCO_3 + 2Al(OH)_3 + 3SiO_2 + H_2O}\end{aligned} \quad (7)$$

(2) Reactions between CO_2 and basaltic/ultramafic minerals in the subsurface. In carbon mineralization, CO_2 reacts with minerals rich in Ca and Mg to form carbonates, such as calcite ($CaCO_3$), magnesite ($MgCO_3$), and dolomite ($CaMg(CO_3)_2$). Some representative reactions are shown as Eqs. (8)–(12):

Wollastonite:

$$\mathrm{CaSiO_3 + CO_2 \rightarrow CaCO_3 + SiO_2} \quad (8)$$

Olivine:

$$\mathrm{Mg_2SiO_4 + 2CO_2 \rightarrow 2MgCO_3 + SiO_2} \quad (9)$$

Pyroxenes:

$$\mathrm{CaMgSi_2O_6 + 2CO_2 \rightarrow CaMg(CO_3)_2 + 2SiO_2} \quad (10)$$

Serpentine polytypes:

$$\mathrm{Mg_3Si_2O_5(OH)_4 + 3CO_2 \rightarrow 3MgCO_3 + 2H_2O + 2SiO_2} \quad (11)$$

Brucite:

$$\mathrm{Mg(OH)_2 + CO_2 \rightarrow MgCO_3 + H_2O} \quad (12)$$

(3) Reaction between CO_2 and industrial wastes. Some alkaline solid wastes (e.g., steel slag, fly ash, cement and concrete waste, red mud, etc.) contain CaO, MgO, $Mg(OH)_2$, $Ca(OH)_2$, $CaSiO_3$, C-S-H (calcium silicate hydrate), $NaAl(OH)_4$, etc., which can react with CO_2 to form carbonates, as shown in Eqs. (13)–(19).

$$\mathrm{CaO + CO_2 \rightarrow CaCO_3} \quad (13)$$

$$\mathrm{MgO + CO_2 \rightarrow MgCO_3} \quad (14)$$

$$\mathrm{Mg(OH)_2 + CO_2 \rightarrow MgCO_3 + H_2O} \quad (15)$$

$$\mathrm{Ca(OH)_2 + CO_2 \rightarrow CaCO_3 + H_2O} \quad (16)$$

$$\mathrm{CaSiO_3 + CO_2 \rightarrow CaCO_3 + SiO_2} \quad (17)$$

$$\mathrm{C\text{-}S\text{-}H + CO_2 \rightarrow CaCO_3 + H_2O + SiO_2} \quad (18)$$

$$\mathrm{2NaAl(OH)_4 + CO_2 \rightarrow Na_2CO_3 + 2Al(OH)_3 + H_2O} \quad (19)$$

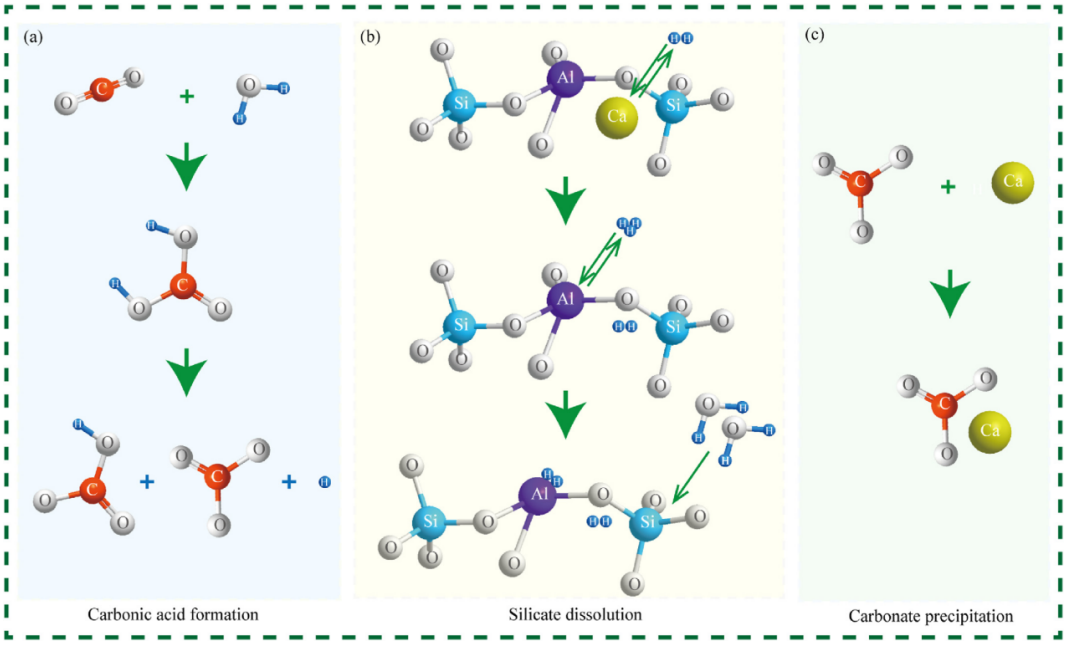

Fig. 3 Schematic diagram of carbon mineralization process (Cao et al., 2024)

3 CO_2 mineralization by aluminosilicates in sandstone

Aluminosilicates, which consist of aluminum (Al), silicon (Si), and oxygen (O) in their structure, play a crucial role in the composition, diagenesis, and overall properties of sandstones, which commonly serve as composing rocks of CO_2 storage formations of large-scale CGUS projects (McGrail et al., 2017; White et al., 2020). The CO_2 mineralization process of aluminosilicates, as a crucial step in geological CO_2 sequestration, contributes to the safe storage of CO_2.

3.1 Principles of mineralogy

Sandstones primarily contain the following aluminosilicates: 1) Feldspars (Na-feldspar, K-feldspar, Ca-feldspar, etc.)(Ennis-King and Paterson, 2007; Lindeberg and Wessel-Berg, 1997) . These are the most abundant aluminosilicates in many sandstones, especially in arkosic and lithic arenites. 2) clay minerals (e.g., kaolinite, illite, smectite, chlorite, etc.). Clay minerals are formed from the weathering of feldspars and other unstable minerals. Clays are key diagenetic products in sandstone. 3) micas (muscovite, biotite). Though less common, micas sometimes contribute to the aluminosilicate content in sandstone. Aluminosilicates are fundamental to sandstone petrology, affecting texture, diagenesis, and reservoir behavior (Knauss et al., 2005). Their presence and transformation determine whether a sandstone becomes a good hydrocarbon reservoir or a tight, impermeable rock.

For sandstone formations that typically contain aluminosilicates, if quartz content in sandstone is high, and contents of anorthite and illite are low, the CO_2-brine-sandstone interaction is expected to be limited, and the contribution of mineral trapping to overall CO_2 trapping becomes low (Tempel and Harrison, 2000). However, if the sandstone formation contains large amounts of reactive minerals like anorthite and illite, the CO_2-brine-sandstone interaction will become obvious. A previous study has demonstrated that though most aluminosilicates have relatively low dissolution rates, anorthite and illite have higher dissolution rates and contribute to CO_2 mineralization within relatively short reaction time (Geloni et al., 2011). Sensitivity analysis showed that anorthite and illite facilitate more CO_2 mineralization than other aluminosilicates, with anorthite and illite showing 0.68 and 0.46 correlation coefficients with CO_2 mineral trapping, respectively. Also, another study discovered that anorthite and illite dissolve better at high temperatures (higher than 80 °C). Therefore, if a sandstone formation contains high volume fractions of anorthite and illite and the formation temperature is high, the mineral trapping of CO_2 can be observed within a short time scale (Alkan et al., 2010; Zheng et al., 2010). The mineral alteration observed in the experiment is shown in Fig. 4.

3.2 Experimental and numerical simulation studies

The process of CO_2 mineralization by aluminosilicates has been widely studied by both experimental and numerical approaches. Experiments were performed using samples from a glauconitic sandstone aquifer in the Alberta Sedimentary Basin, to validate results obtained with a batch geochemical model. The laboratory experiments were performed for one month at 105 °C and 9 MPa CO_2 pressure to accelerate the reaction rate, because the kinetics of aluminosilicate reactions at room temperature are generally slow to observe any significant CO_2 consumption in a reasonable length of time (Black et al., 2015). Though the temperature and CO_2 pressure were raised, the experimental results indicated that very little CO_2 was trapped through reaction with aluminosilicate minerals within one month (Gunter et al., 1993). Extending the model to the field, it was found by Gunter et al. (1993) that the CO_2 trapping reactions by aluminosilicates would take hundreds of years to

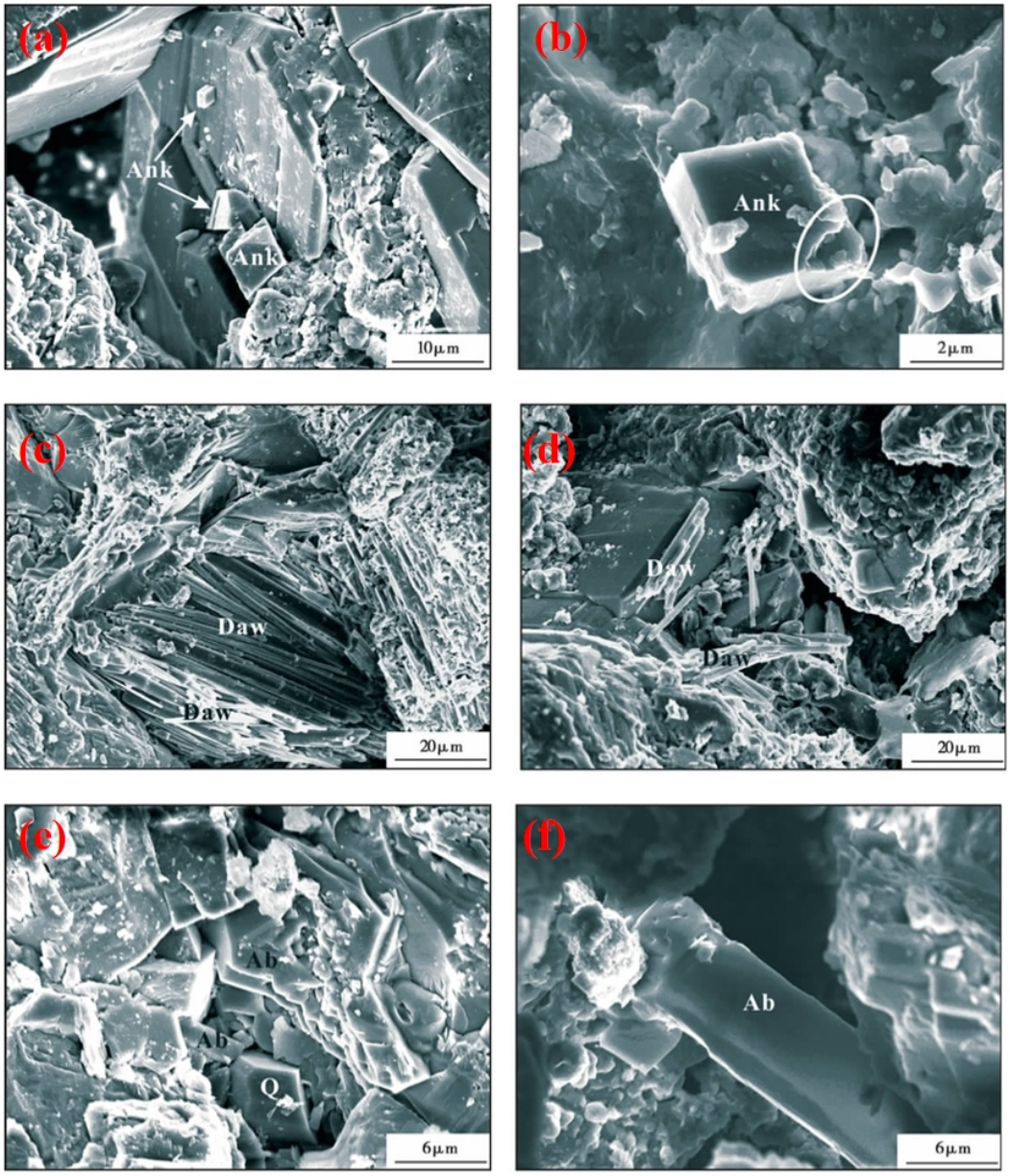

Fig. 4 Alteration of sandstone minerals under the action of CO_2: (a) ankerite (Ank) before reaction; (b) ankerite (Ank) after reaction; (c) dawsonite (Daw) before reaction, Q represents quartz; (d) dawsonite (Daw) after reaction; (e) albite (Ab) before reaction; (f) albite (Ab) after reaction (Yu et al., 2012)

complete after the formation water was equilibrated with CO_2 at the temperature of the aquifer (54 °C) and at the proposed CO_2 injection pressure (26 MPa). Even under favorable conditions where aluminosilicate mineral dissolution and subsequent carbonate mineral precipitation are likely to occur (i.e., pH 4.5 to 6, fluid flow velocity less than 5 m/year, and 50–100 years or more after the start of injection), it will still take 200 to 2000 years for conversion of 60–90% of injected CO_2 into solid carbonates when the reservoir rock has a sufficient volume fraction of divalent cation-bearing aluminosilicate minerals (Izgec et al., 2017; Izgec et al., 2008).

White et al. performed a numerical assessment of the CO_2 storage potential at a site located in the Colorado Plateau of central Utah, utilizing ChemTOUGH to simulate the injection of CO_2 into sandstone formations (White et al., 2020). The results of the study indicated that approximately 21% of the injected CO_2 would be stored in mineral form after 1,000 years, while 52% would dissolve in water as a gas, and 17% would escape. Additionally, the calculations conducted by (Wang et al., 2016) illustrated the evolution of injected CO_2 within geological formations, as depicted in Fig. 5. Xu et al. used geochemical models to study the chemical reaction between sandstone aquifer and CO_2, and found that the reaction between sandstone and CO_2 will lead to the precipitation of secondary carbonate minerals such as dawsonite, calcite, muscovite, siderite, magnesite, etc., resulting in a decrease in porosity and permeability of

the CO_2 storage formation (Xu et al., 2008). Li et al. studied the water-CO_2-rock interaction between a mixture of albite, dolomite, orthoclase, quartz and anorthite (mimicking typical sandstone compositions) and natural aquifer water (obtained from the Springerville-St (Li et al., 2015). Johns CO_2 field). They observed precipitation of kaolinite when the CO_2 concentration was 0.03 mol/kg, and precipitation of dawsonite when the CO_2 concentration was 0.07 mol/kg. Vermolen et al. added CO_2 to rock samples saturated with formation water until the concentration of CO_2 reached 1 mol/kg. They observed that the reduction of pH caused the formation of alunite, and some of the precipitated kaolinite was dissolved. This study exhibits the significant effect of CO_2 concentration and aquifer pH on mineral dissolution and precipitation (Vermolen et al., 2009). Knauss et al. conducted a numerical simulation to study geochemical interaction between injected CO_2 and sandstone at Bunter CO_2 storage formation, North Sea, and the simulation results predicted precipitation of $CaCO_3$, which caused a 20% porosity reduction of the sandstone (Knauss et al., 2005).

In summary, previous studies have shown that CO_2 storage in most sandstone formations requires at least 200 years for the mineral trapping by aluminosilicates to have a noticeable contribution to the overall CO_2 trapping.

4 CO_2 mineralization by basalts

Basalt, which is widely distributed across the globe, as demonstrated in Fig. 6, presents an alternative approach for the mineralization and storage of CO_2. The technology for CO_2 mineralization and storage in basalt has garnered significant attention owing to its high level of safety, long-term stability, and potential for large-scale implementation. Basalt is rich in magnesium-bearing and iron-bearing minerals, such as olivine and pyroxene, which can undergo CO_2-water-rock interactions to form stable carbonate minerals, including magnesite and calcite (Chaïrat et al., 2007). This process facilitates the long-term fixation of CO_2(Gudbrandsson et al., 2014). In comparison to traditional storage methods employing saline aquifers or depleted oil and gas reservoirs, basalt mineralization storage provides several advantages, including accelerated reaction rates, increased storage capacity, and exceptionally low leakage risks. These attributes render it suitable for addressing large-scale CO_2 emission reduction efforts (Van Herk et al., 1989).

4.1 Reaction rates of different basalt minerals

Basalt comprises a diverse array of minerals, including olivine, plagioclase, pyroxene, basalt glass, serpentine, and crystal basalt (Cao et al., 2024). The release rates of metal ions from these different mineral components exhibit significant variations (Snæbjörnsdóttir et al., 2020). The dissolution behavior of basaltic minerals is a critical factor influencing the efficiency of CO_2 geological storage, with the kinetics of these processes being contingent upon the crystal structures of the minerals involved (Mcgrail et al., 2003). As the predominant mineral in magnesium-iron basalt, olivine is characterized by a rapid dissolution rate (Noack et al., 1993). Under acidic conditions, the dissolution of olivine adheres to a proton-promoted mechanism, whereby surface-coordinated Mg^{2+} ions are preferentially substituted by H^+ ions, resulting in the destabilization of the silicate framework (Gislason and Oelkers, 2003). Recent investigations have observed the formation of a 2–5 nm thick amorphous silica layer on the mineral surface during the initial stages of dissolution; this layer hinders the transport of subsequent reactants, leading to an exponential decline in the dissolution rate over time (Aradóttir et al., 2012; Golubev et al., 2005). Notably, the presence of Fe^{2+} in olivine can induce localized microbattery effects during dissolution, giving rise to pitting phenomena, with dissolution rate variations in different regions reaching up to 10-fold differences (Lasaga, 1984; Munz et al., 2012; Siegel, 1984).

The dissolution behavior of plagioclase minerals demonstrates a marked dependence on compositional differences, with the dissolution rate of anorthite being 1–2 orders of magnitude faster than that of albite (Gudbrandsson et al., 2008). This disparity primarily arises from variations in the activation energy linked to the release of Al^{3+} from diverse structural environments (Oelkers, 2001). Within the neutral pH range, the dissolution of plagioclase is governed by the breakage of Al-O bonds, and its rate is closely correlated with the coordination number of Al (Kampman et al., 2009). The presence of organic ligands in the fluid phase, such as oxalic acid, has been shown to enhance the dissolution rate of anorthite by 5–8 times through the formation of complexes with Al^{3+}. The dissolution of pyroxene minerals exhibits characteristics akin to chain silicates, which are associated with the exposure of Si-O chains (Gautier et al., 2001). In CO_2-saturated aqueous solutions, the Fe^{2+} released during the dissolution of pyroxene may participate in carbonate precipitation, establishing a self-catalytic cycle that results in long-term dissolution rates being 30–50% higher than those observed in short-term experimental assessments (Hänchen et al., 2006).

Basalt glass, which forms as a result of rapid cooling during volcanic eruptions, exhibits significantly distinct dissolution behavior when compared to its crystalline counterparts (Carroll and Knauss, 2005). Its amorphous structure results in dissolution rates that are 10–100 times faster than those of crystallized minerals with similar compositions, and it does not display crystal face anisotropy. The dissolution process results in the formation of a weathering layer characterized by depth-dependent gradual changes in chemical composition (Song et al., 2023). As a representative hydrous silicate, serpentine experiences dissolution controlled by the oxidation of Fe^{2+}, with dissolution rates in oxidizing conditions being 1–2 orders of magnitude greater than those in reducing conditions. The unique structure of glassy basalt promotes the development of a network of micro-cracks during fluid penetration, effectively increasing the reactive surface area over time and exhibiting "self-accelerating" dissolution characteristics (Lehmann and Possinger, 2020; Loubser, 2013).

The layered structure of serpentine minerals results in pronounced anisotropy in dissolution rates, with the rate perpendicular to the [001] direction being 10–20 times greater than that measured parallel to this direction (Goldberg and Slagle, 2009; Yang et al., 2016) . Under alkaline conditions, the preferential leaching of interlayer Mg^{2+} can lead to mineral curling and delamination, thereby increasing the reactive interface (Awad

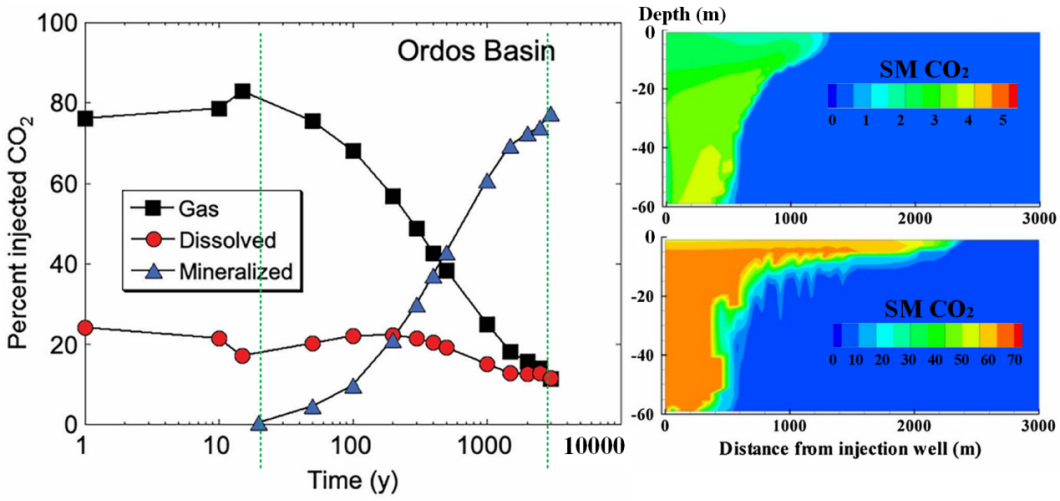

Fig. 5 The evolution of the injected CO_2 in the formation (Wang et al., 2016)

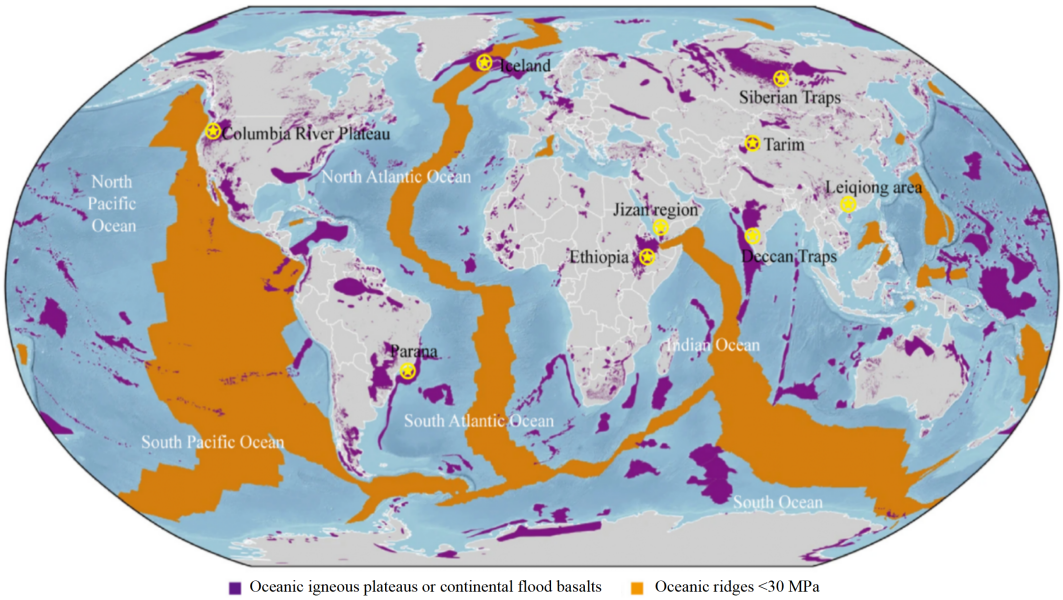

Fig. 6 Locations of basalts (Snæbjörnsdóttir et al., 2020)

et al., 2000). Recent research has identified that magnesium silicate nanoparticles generated during the dissolution of serpentine may act as nucleation sites for carbonate precipitation, thereby establishing a coupled dissolution-precipitation mechanism (Beaulieu et al., 2010; Maher and Chamberlain, 2014).

4.2 Factors influencing the reaction rate of basalt

The dissolution kinetics of basalt minerals are governed by a combination of environmental factors, with temperature, pressure, pH, and fluid flow conditions serving as the most critical control parameters (Rani et al., 2013). Temperature affects the dissolution process by modifying both the reaction activation energy and the diffusion coefficient, as quantitatively described by the Arrhenius equation (Zhang et al., 2022). For common basaltic minerals such as olivine, the activation energy for dissolution ranges from 60 to 80 kJ/mol, resulting in an increase in dissolution rate of 2–3 times for each 10°C rise in temperature (Awad et al., 2000). Under high-pressure conditions (>10 MPa), the solubility of CO_2 increases non-linearly with pressure. For example, increasing the pressure from 1 MPa to 10 MPa can enhance the dissolution rate of basalt glass by 5–8 times, primarily due to the increased concentration of carbonates and improved fluid permeability (Choubineh et al., 2019). Furthermore, the dissolution behavior under supercritical CO_2 ($scCO_2$) conditions is characterized by a distinct kinetic inflection point around 7.38 MPa and 31.1°C, where the carbonate product layer formed on the mineral surface is thinner (<50 nm) and more porous, thereby facilitating sustained chemical reactions (Rosso and Rimstidt, 2000).

pH is a critical variable controlling the dissolution mechanism. In acidic conditions, the dissolution process is predominantly governed by a proton-promoted mechanism (Tester et al., 1994). In neutral to weakly alkaline conditions, the direct attack of water molecules on the silicate bonds becomes the rate-

limiting step (Iglauer and Al-Yaseri, 2021). In strongly alkaline environments, the nucleophilic cleavage of Si-O-Si bonds by OH^- further enhances the dissolution rate (Abdulelah et al., 2021). The pH versus dissolution rate curve for basalt minerals typically exhibits a "U" shape, with minimum dissolution rates occurring in the pH range of 5 to 7 (Metz et al., 2005). Fluid dynamic conditions modulate the dissolution process by influencing mass transport and surface renewal. When the Reynolds number (Re) exceeds 10^4, the boundary layer thickness can decrease to 10–100 μm, resulting in a 3–5 fold increase in the dissolution rates of plagioclase. Microfluidic experiments have corroborated that minor variations in flow rates at the pore scale (50–500 μm) can lead to significant changes in the morphology of the dissolution front, shifting from uniform weathering to finger-like channel growth (Hänchen et al., 2006; Jarvis et al., 2009).

Coupling effects among various environmental fields have emerged as a key focus of contemporary research (Ali et al., 2019). The synergistic interaction between temperature and pH is evident; at low temperatures, the pH effect dominates, while the influence of temperature becomes more pronounced at higher temperatures (Voigt et al., 2021). The coupling of pressure and flow is noted in the stability changes of fluid pathways under high confining pressures; specifically, a confining pressure of 10 MPa can maintain micro-cracks in an open state, effectively increasing the reactive surface area by 2–3 times (Ali et al., 2023). Recently developed in situ characterization techniques facilitate real-time monitoring of multiple parameters, thereby revealing critical transition points in mineral dissolution mechanisms.

The spatial and temporal heterogeneity of environmental conditions gives rise to non-linear characteristics in dissolution behavior (Bandstra and Brantley, 2008a). Field monitoring data indicate that the dissolution rates of minerals in basalt aquifers decrease along fluid flow pathways, with rates in the first 10 meters being 1–2 orders of magnitude higher than those at 50 meters (Jeschke and Dreybrodt, 2002; Wells et al., 2017). This scale effect is challenging to replicate in laboratory settings and is primarily extrapolated through reaction-transport models. Long-term experiments have revealed an "aging" phenomenon in mineral dissolution, with rates during the initial phase being 5–10 times higher than those observed during the stable phase, closely associated with the development of a passivation layer on the surface (Seyama et al., 1996; Yekeen et al., 2020).

Environmental factors also play a decisive role in the formation of secondary minerals (Prigiobbe et al., 2009). In low-temperature conditions, an amorphous silica product layer is readily formed, while high-temperature environments promote the precipitation of layered silicates, such as montmorillonite (Blum and Lasaga, 1988). These secondary phases alter the effective reactive surface area and mass transport pathways, providing feedback that regulates the dissolution rates of primary minerals (Al-Yaseri et al., 2021b). Under conditions favorable for CO_2 storage, the precipitation of secondary carbonates can locally elevate pH, creating a self-regulating mechanism that stabilizes dissolution rates over time (Giammar et al., 2005).

4.3 Typical basalt carbon sequestration projects

Multiple demonstration projects worldwide have validated the feasibility of CO_2 mineralization and storage technology, with the CarbFix (Iceland), Wallula (USA), SOLVE (Norway), and CO_2-DISSOLVED (France) projects representing innovative technological approaches across different geological scenarios (Pogge von Strandmann et al., 2019). The CarbFix project, implemented at the Hellisheidi geothermal field in Iceland, is the largest in situ basalt mineralization project globally. Its core technological breakthrough involves the CO_2-geothermal water mixed injection strategy (molar ratio of 1:3), which facilitates the mineralization reaction through both the thermal energy and dissolved ions (Ca^{2+} and Mg^{2+} concentrations >100 mg/L) of geothermal fluids (Schwartz, 2022). Monitoring data indicates that the injected CO_2 achieved a mineralization rate exceeding 95% in less than two years, significantly faster than early predictions, attributed to the project's innovative stepped injection scheme (Gislason et al., 2010). The strategy begins with a low CO_2 proportion (10%) to activate the mineral surface and gradually increases to 50%, thereby continuously renewing the reaction interface (Schwartz, 2018; Sigfússon et al., 2018). Geochemical tracing confirmed that the primary mineralization products are predominantly magnesite and calcite, uniformly distributed without localized blockage (McGrail et al., 2017). Additionally, the project developed a real-time microseismic monitoring system with a positioning accuracy of 10 meters, successfully providing early warnings for three microfracture activities induced by carbonate precipitation (Ajoma et al., 2020). The picture showing the conversion of CO_2 into calcite in the CarbFix project is shown in Fig 7.

The Wallula deep basalt demonstration project in the United States adapted technology to the characteristics of continental basalt, with its core innovation being the use of a supercritical CO_2 injection mode (Schwartz, 2018). The project operates at depths of 800–1000 meters in the Columbia River basalt group and enhances the release rate of Fe^{2+} by five times through the addition of 0.1 mol/L sodium citrate as a complexing agent, thereby promoting the precipitation of iron-magnesium carbonates (Gíslason et al., 2018). Observations from an underground fiber optic sensing (DTS/DAS) network indicated a 15% increase in wave velocity in the near-well region (<30 m) six months post-injection, reflecting mineral fill effects (White et al., 2020). Notably, the project employed a pulsed injection strategy (two months of injection followed by one month of suspension), alleviating the permeability decline caused by carbonate precipitation. This approach provides critical insights for basalt reservoirs with high clay content. Monitoring has shown that the mineralization rate stabilizes at 70–80%, with no leakage detected (Matter et al., 2011).

The SOLVE project in Norway explores a saline formation-mineral co-storage technology in offshore basalt formations in the North Sea. Its distinguishing feature is the development of a self-adjusting acid system, which dissolves minerals at low pH (<4) and automatically demulsifies to release CO_2 as the pH increases (>6), achieving spatial separation of dissolution and precipitation processes (Johnson et al., 2005). Project data

Fig. 7 Evidence of CO_2 mineralization in the CarbFix project (Snæbjörnsdóttir et al., 2017)

demonstrate that this technology improves CO_2 reach efficiency by 40%, with a mineralization rate of 50 kg/m^3 per year (Tsakiroglou et al., 2018). The project also pioneered a remote monitoring technology based on nano-magnetic particles, allowing for the inversion of carbonate distribution (accuracy ±5%) by monitoring the electromagnetic response changes of injected Fe_3O_4·SiO_2 nanoparticles (50 nm in diameter) (Han et al., 2019; Miocic et al., 2014).

The CO_2-DISSOLVED project in France represents a shallow low-temperature mineralization approach, where CO_2 is dissolved in groundwater and injected into a basalt aquifer located 150 meters deep in the Paris Basin (Luhmann et al., 2017). The project's innovation lies in utilizing the natural iron minerals (hematite, magnetite) in the aquifer as catalysts, accelerating carbonate nucleation through the Fe^{2+} cycle (Gíslason et al., 2018). Monitoring results indicate that although low temperature (25°C) initially slows down mineralization (30% after two years), a self-accelerating characteristic emerges in the later stages, with a mineralization rate reaching 90% after five years. The low-cost monitoring technology developed by the project serves as a model for small-scale community-level storage (Rahman et al., 2022).

5 CO_2 mineralization by industrial wastes

CO_2 mineralization by industrial wastes is recognized as a promising emission reduction technology with significant potential for large-scale CO_2 sequestration applications, as illustrated in Fig. 8 (Zhang et al., 2024). CO_2 mineralization by industrial wastes refers to a process that mimics the natural mechanism of CO_2 mineral absorption, utilizing naturally occurring ores or solid waste that contain alkaline or alkaline earth metal oxides to produce stable solid carbonates via carbonation reactions (Liu et al., 2025; Wang et al., 2025). Industrial solid waste rich in calcium and magnesium oxides, such as fly ash, slag, carbide slag, and construction debris, possesses considerable CO_2 mineralization potential due to its large annual production and high reactivity (Xu and Mo, 2024). The CO_2 mineralization by industrial wastes is typically accomplished through a non-in-situ mineralization process. This methodology involves collecting reactive industrial wastes (e.g., calcium-rich fly ash, calcium- and magnesium-rich tailings), grinding them into fine particles, and facilitating their reaction with CO_2 in a controlled industrial environment (Raganati et al., 2024). Following the reaction between industrial waste and carbon dioxide, the resultant material is placed in above-ground underground spaces, such as coal mine goaf areas, for permanent disposal (Xie et al., 2015).

5.1 Mineralization methods

Industrial solid waste represents a significant source of raw materials for CO_2 mineralization and storage, with treatment technologies categorized into direct and indirect methods based on their reaction mechanisms and process characteristics (Ramasenya et al., 2025a). The direct mineralization method facilitates carbon fixation through the direct reaction between CO_2 and the alkaline components present in solid waste, operating via a three-step reaction mechanism that involves water (Morales-Flórez et al., 2011). Studies on the direct mineralization of steel slag have demonstrated that a carbonation rate exceeding 80% can be achieved within 24 hours under standard conditions (Grünhäuser Soares et al., 2022). Recent advancements in this technology have employed mechanical activation to enhance the specific surface area to 15–20 m^2/g, resulting in a significant increase in the carbonation rate by 3–5 times (Ren et al., 2020). The utilization of supercritical CO_2 further amplifies the reaction rate by one to two orders of magnitude when compared to gas-phase CO_2 conditions (Duan et al., 2024; Rahmani, 2020).

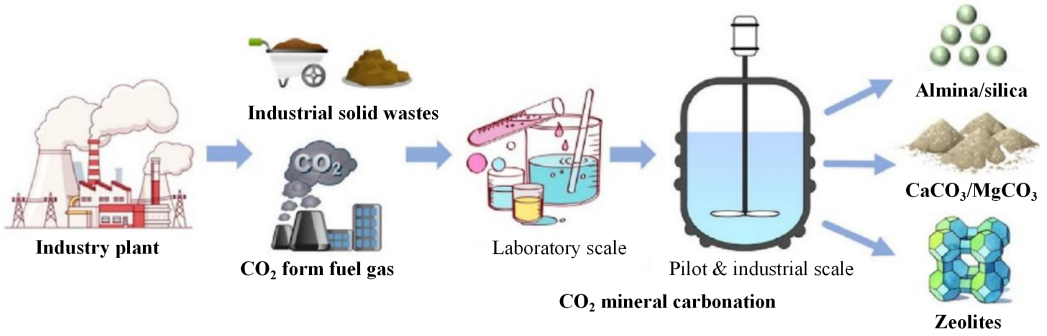

Fig. 8 Schematic diagram of CO_2 mineralization by industrial wastes (Chen et al., 2021)

Dry mineralization technology has gained considerable attention due to its operation without a liquid phase medium. This process typically functions under conditions of 30–70% relative humidity and temperatures ranging from 50 to 200°C, with the reaction dictated by surface adsorption-diffusion mechanisms (Cárdenas-Escudero et al., 2011). Recent research indicates that the carbonation depth of steel slag exposed to a CO_2 atmosphere increases parabolically over time, and steam activation pretreatment can enhance the reaction rate by 2–3 times (Ebrahimi et al., 2018). Conversely, wet mineralization occurs within the liquid phase and can be subdivided into three pathways depending on pH conditions: acidic, neutral, and alkaline. Although acidic wet methods facilitate rapid reaction rates, they encounter challenges related to equipment corrosion and subsequent neutralization procedures. Neutral wet methods stabilize the pH at 7–8 by incorporating buffers, achieving carbonation rates of 60–80% under mild conditions. Alkaline wet methods, while ensuring thorough reactions, necessitate strict controls to prevent the formation of silicate gels that could obstruct the reaction (Wang et al., 2024). In terms of reactor design, fluidized bed reactors exhibit favorable adaptability for both dry and neutral wet methods, while high-pressure reactor systems are better suited for acidic wet processes (Rahmani, 2018).

The indirect mineralization method utilizes a two-stage process involving medium extraction and precipitation separation. The acidic extraction typically involves the use of HCl, H_2SO_4, or organic acids to dissolve metal ions from solid waste at pH levels between 2 and 4 (Li et al., 2023). In contrast, the alkaline extraction method employs ammonium salts such as NH_4Cl through ion exchange to extract Ca^{2+}/Mg^{2+} ions, achieving a metal ion recovery rate of 85% under optimized conditions. Following extraction, the solution is treated with CO_2 for carbonation, where controlling the saturation index between 0.5 and 1.5 ensures the production of high-purity carbonate products (Xu et al., 2024a).

The industrial application of these various technological pathways reflects differentiated development trends. The direct method, owing to its simplicity, has achieved commercialization within the construction materials sector, exemplified by Canada's CarbonCure technology, which incorporates steel slag mineralization products as concrete additives, sequestering 25 kg of CO_2 per cubic meter of concrete (Ebrahimi et al., 2017). The indirect method, on the other hand, offers advantages for the production of high-value-added products. Dry mineralization shows promise for in-situ storage in solid waste landfills, while wet mineralization is more appropriate for centralized treatment (Liu et al., 2021). From a techno-economic perspective, both direct and dry methods present lower normalized costs but comparatively limited carbonation rates; conversely, indirect and wet methods, although associated with higher costs, can achieve carbonation rates exceeding 90% alongside high product purity (Kaithwas et al., 2012).

5.2 Mineralization characteristics of different solid waste materials

Industrial solid waste utilized for CO_2 mineralization and storage primarily includes steel slag, fly ash, phosphogypsum, and tailings, all of which are significant sources of raw materials due to their high content of alkaline components such as Ca and Mg. The mineralogical characteristics and chemical composition of these solid wastes substantially influence their mineralization behavior and storage efficiency.

Steel slag is regarded as the most promising mineralization feedstock, owing to its high alkalinity and abundant free CaO, which confer excellent CO_2 fixation capabilities. Research indicates that the theoretical CO_2 storage potential of converter steel slag can reach 200–300 kg/t under standard conditions, with dicalcium silicate and free CaO serving as the primary active components. The nano-sized $Ca(OH)_2$ clusters present on the surface of steel slag particles act as preferential sites for carbonation reactions (Xu et al., 2024a). Mechanical activation enhances the specific surface area of steel slag, thereby improving its carbonation efficiency. Notably, the 2–5% Fe_2O_3 content in steel slag exhibits catalytic effects, promoting electron transfer through the Fe^{2+}/Fe^{3+} cycle during the wet mineralization process, which in turn increases the precipitation rate of calcium carbonate (Chen et al., 2021). However, the presence of heavy metals, such as Cr and Pb, in steel slag may leach under acidic mineralization conditions, necessitating the maintenance of pH levels above 6 to ensure environmental safety. The carbonation reaction process of steel slag is illustrated in Fig. 9.

The mineralization behavior of fly ash is closely linked to its glassy phase content (Yao et al., 2024). The high-calcium glassy phase in circulating fluidized bed (CFB) ash exhibits rapid dissolution characteristics, wherein the release of Al^{3+}

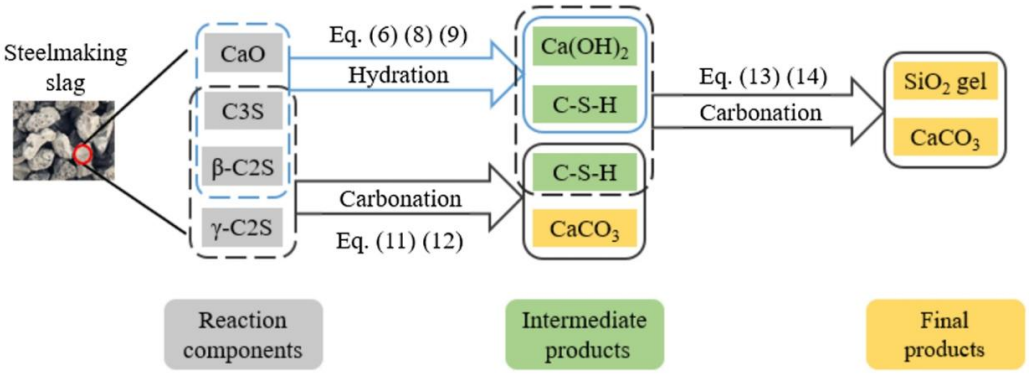

Fig. 9 The reaction processes of calcium component in steelmaking slag (Xu et al., 2024a)

ions competes with Ca^{2+} to form calcium aluminum garnet, thereby reducing CO_2 fixation efficiency (Peng and Xia, 2024; Singh et al., 2024). Selective extraction of Ca^{2+} using an NH_4Cl solution can achieve carbonation rates exceeding 75% (Luo et al., 2024). The presence of unburned carbon in fly ash has a dual effect: it acts as a nucleation site to promote carbonate precipitation while also adsorbing CO_2 molecules, hindering gas-solid contact. Microwave oxidation pretreatment can reduce the unburned carbon content to below 1%, while also relaxing the glassy structure to enhance the dissolution rate (Luan et al., 2024; Niu et al., 2024; Xia and Peng, 2024).

The mineralization of phosphogypsum necessitates conversion through an ammonium salt medium. Impurities present in phosphogypsum compete with Ca^{2+} to form precipitates, which consequently decreases the purity of calcium carbonate to 80–85% (Szczygiel and Jagoda, 2013). The addition of sodium polyacrylate can selectively inhibit the co-precipitation of impurities, resulting in a product purity exceeding 95%. Importantly, the $(NH_4)_2SO_4$ solution generated as a byproduct from this process can be recovered through membrane separation, achieving an ammonium ion recycling rate greater than 90% (Zhang et al., 2022). The mineralization characteristics of metal tailings are constrained by the stability of their silicate structures. Olivine tailings require strong acidic conditions with pH < 3 for effective dissolution, which can lead to silica gel encapsulation issues (Tian, 2002). Conversely, high-silica tailings must undergo alkaline fusion activation to disrupt the Si-O network, thereby enhancing their CO_2 fixation potential (Xie et al., 2022).

The reaction of CO_2 with wellbore cement can lead to cement degradation and an increased risk of leakage (Gan et al., 2020). This reaction can occur rapidly over a short period, and its changes, as depicted in CT scans, are illustrated in Fig. 10. When the cement-based materials involved in the CO_2 reaction are derived from construction waste, this process promotes CO_2 mineralization and storage (Kravchenko et al., 2024; Kuoribo et al., 2024). The mineralization of construction waste, such as discarded concrete, exhibits multi-scale characteristics (Teo et al., 2022). Macroscopically, the carbonation reaction progresses inward from the surface; microscopically, the carbonation of C-S-H gel results in a reduction of its Ca/Si ratio from 1.7 to 0.8, forming nanopores that facilitate CO_2 penetration (Tian, 2002; Ravichandran et al., 2024). Additionally, steam curing pretreatment can increase the CO_2 absorption capacity of construction waste (Kaptan et al., 2024; Naguib, 2024; Yuan et al., 2024).

5.3 Factors influencing the iate of mineralization

Industrial solid waste constitutes a significant raw material for CO_2 mineralization and storage, with its reaction efficiency being influenced by multiple factors, including material properties, reaction conditions, and process parameters (Kusin et al., 2024). Regarding material properties, the chemical composition of solid waste determines its theoretical CO_2 storage potential; for instance, steel slag, which contains 10–15% free CaO, demonstrates strong CO_2 fixation capabilities. The mineral phase composition also affects reaction reactivity, with amorphous phases exhibiting greater reactivity compared to crystalline phases (Karishma et al., 2024). Additionally, the specific surface area and pore structure dictate the size of the reactive interface, while mechanical activation can significantly enhance reaction rates (Lee et al., 2021). In terms of reaction conditions, temperature plays a crucial role in the mineralization process by influencing both reaction kinetics and CO_2 solubility. The partial pressure of CO_2 dictates the driving force of the reaction; consequently, increasing the pressure can enhance the carbonation rate of steel slag. pH levels also regulate the reaction pathway, with acidic conditions promoting the leaching of metal ions, whereas alkaline conditions favor the precipitation of carbonates. Furthermore, process parameters such as the liquid-to-solid ratio affect mass transfer efficiency, and stirring intensity determines the thickness of the boundary layer (Tetteh et al., 2021).

To improve the CO_2 mineralization efficiency of solid waste, several enhanced reaction technologies have been developed in recent years, which can be classified into three main categories: physical activation, chemical activation, and process intensification (Senthilkumar et al., 2025). Physical activation techniques increase reaction activity by modifying the physical properties of the solid waste, with mechanical milling being the most commonly employed method. By reducing the particle size of steel slag, the reaction rates can be significantly improved. Microwave activation utilizes dielectric heating to selectively excite polar molecules, thereby relaxing the glassy

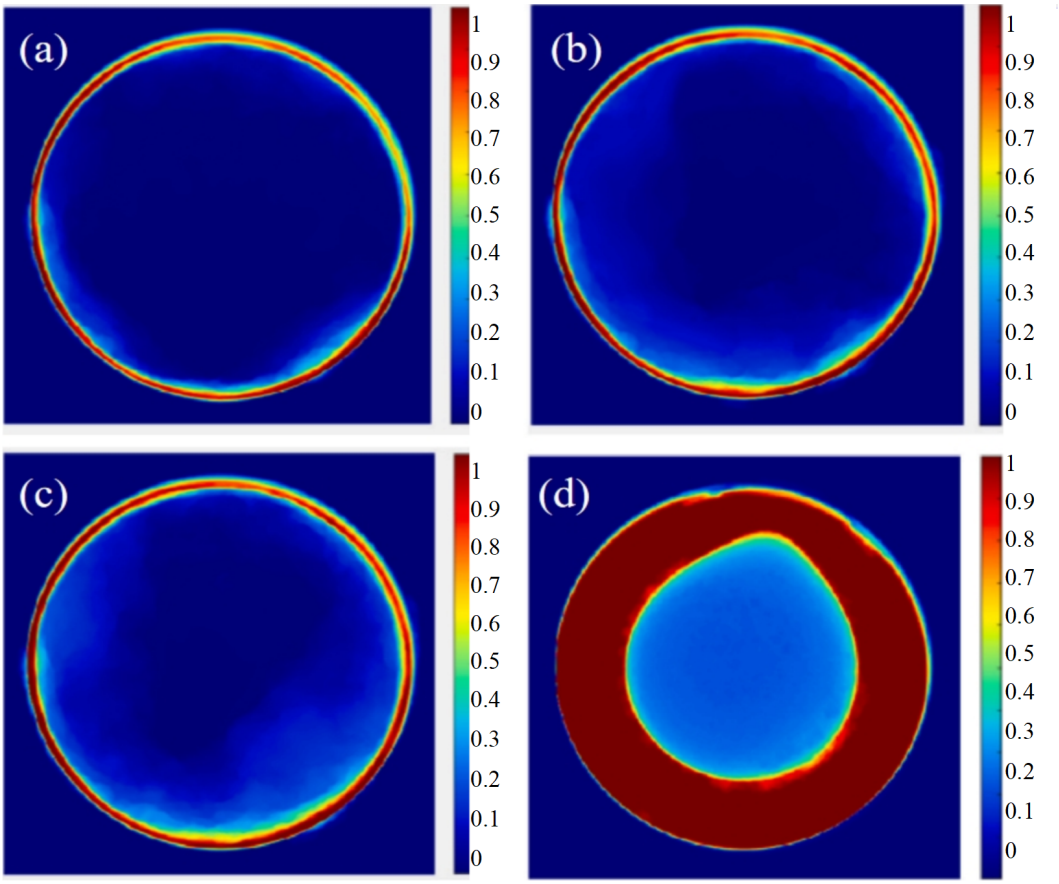

Fig. 10 The alteration area of cement under the action of CO_2 based on post-processing of CT scans: (a) 7 days; (b) 14 days; (c) 28 days; (d) 56 days (Gan et al., 2025)

structure of fly ash and enhancing its dissolution rate. Ultrasonic cavitation produces localized high temperatures and pressures, which can continuously refresh the reaction interface and inhibit the formation of passivation layers. Chemical activation techniques modify reaction pathways through the addition of specific reagents. Acidic activation employs HCl, H_2SO_4, or organic acids to dissolve metal ions under pH conditions ranging from 2 to 4, with acetic acid concentrations of 0.5–1 mol/L achieving Ca extraction rates from steel slag exceeding 90%. Catalytic activation involves the introduction of carbonic anhydrase or metal oxides to enhance the hydration reaction rate with CO_2. Process intensification techniques improve efficiency by optimizing reactor design and operational conditions. Supercritical CO_2 technology leverages the unique physical properties of $scCO_2$, resulting in mass transfer rates that are one to two orders of magnitude higher than those observed with gas-phase CO_2 (Navarro et al., 2025).

5.4 Characteristics and applications of mineralized products

The mineral phase composition of solid waste CO_2 mineralization products is primarily determined by the type of raw materials and the conditions under which mineralization occurs. Steel slag-based mineralization products predominantly consist of calcite, with minor amounts of aragonite and vaterite present. In contrast, the products derived from fly ash typically include hydrotalcite-like minerals, while the transformation products of phosphogypsum yield high-purity calcite (Ramasenya et al., 2025a). The mechanical properties of these mineralization products directly influence their value in engineering applications. The compressive strength of steel slag-based products can reach 50–80 MPa, comparable to that of ordinary Portland cement. In comparison, although fly ash products exhibit lower strength, they demonstrate superior toughness (Wang et al., 2025). This difference can be attributed to variations in their microstructural characteristics: the calcium carbonate crystals in steel slag products form a rigid framework through tight interlocking, whereas the hydrotalcite phase in fly ash products possesses a layered structure that allows for energy absorption through slip (Jang et al., 2025). Additionally, the dissolution rate of steel slag products is lower than that of limestone, which is attributed to the calcium silicate protective layer formed on their surfaces. Notably, by carefully controlling the degree of carbonation, self-healing materials can be synthesized, enabling the repair of micro-cracks through the continued carbonation of unreacted $Ca(OH)_2$ in humid environments (Nakao et al., 2025).

Within the construction materials sector, mineralization products are primarily utilized as aggregates or additives. For instance, incorporating steel slag mineralization products into

concrete has been shown to enhance compressive strength. Construction materials formulated with fly ash products possess a density that is only 60–70% of that of traditional products, as well as a 30% reduction in thermal conductivity. In the chemical industry, high-purity calcium carbonate products find applications in the plastics, paper, and coatings sectors. In environmental engineering, mineralization products act as passivators for the remediation of heavy metal-contaminated soils. Furthermore, nano-structured magnesium carbonate has exhibited promising application potential in high-end fields such as pharmaceutical carriers and catalyst supports (Liu et al., 2024).

6 Enhanced mineralization techniques

The efficiency of CO2 mineralization and storage technology, as well as process control, is heavily dependent on the pH environment and the catalytic mechanisms within the reaction system. Research has demonstrated that precise regulation of pH typically maintained within the range of 2 to 10 combined with the use of efficient catalysts, can significantly enhance both the dissolution rate of silicate minerals (such as olivine and serpentine) and the efficiency of carbonate precipitation (Phukan et al., 2021).

During the acidic enhanced dissolution stage (pH<5), both inorganic acids (e.g., HCl and H_2SO_4) and organic acids (e.g., oxalic and citric acids) facilitate the leaching of Mg^{2+} and Ca^{2+} ions through proton-promoting mechanisms. For example, a 0.5 M oxalic acid solution at 80°C can enhance the dissolution rate of olivine by 8-10 times (McGrail et al., 2017). However, excessive acidification (pH<2) may lead to the collapse of the silicate tetrahedral structure, thereby inhibiting the ongoing reaction. To mitigate this issue, novel buffering systems have been developed to maintain an optimal pH window of 4-6, which ensures effective dissolution kinetics while preventing structural degradation of the minerals. Experimental results confirm that this strategy increases the magnesium extraction rate from serpentine by 40%.

Significant advancements have also been achieved in catalytic technologies during the alkaline carbonation stage (pH>8). Biomimetic carbonic anhydrase catalysts, designed to mimic the active sites of biological enzymes (specifically the Zn^{2+}-OH^- structure), have successfully lowered the activation energy of the CO_2 hydration reaction from 35.6 kJ/mol to 21.4 kJ/mol, resulting in a reaction rate enhancement of up to 105 times (Flaathen et al., 2010). Additionally, nanometer-sized Ni-Fe bimetallic catalysts (with particle sizes ranging from 5 to 10 nm) facilitate the dehydration of HCO_3^- through surface oxygen vacancies, thereby increasing the nucleation rate of magnesite by three orders of magnitude at 150°C (Squires and Wolf, 2006). The development of pH-responsive smart catalysts is particularly noteworthy; for instance, Fe_3O_4 nanoparticles coated with polydopamine release Fe^{2+} ions under acidic conditions (pH < 6) to enhance mineral dissolution, while serving as nucleation sites for carbonate precipitation in alkaline environments (pH>8). This approach effectively achieves spatiotemporal coupling of the dissolution-precipitation process (Gudbrandsson et al., 2014).

The coupling technology of geothermal systems and CO2 mineralization and storage (Geothermal-CCUS) has garnered significant attention in recent years as an innovative pathway for achieving negative emissions. The core principle of this approach lies in leveraging the thermodynamic properties and chemical composition of geothermal fluids to substantially accelerate the rate of CO2-rock interactions (Maher and Chamberlain, 2014).

When geothermal water is mixed and injected with supercritical CO2 in specific ratios, a synergistic mechanism of ”thermal-chemical-mechanical” enhancement can be established, resulting in mineralization efficiencies that are 3-5 times greater compared to conventional brine injection methods (Morse and Arvidson, 2002; Vriens et al., 2020). The divalent cations present in geothermal water participate in rapid carbonation reactions with dissolved CO2. Experimental data indicate that under conditions of 150°C and 15 MPa, the dissolution rate constant for plagioclase in basalt increases from 10^{-12} mol/(m^2·s) to 10^{-10} mol/(m^2·s), while the precipitation rate of secondary carbonates improves by two orders of magnitude (Moore et al., 2012).

7 Challenges and future directions in CO_2 mineralization

7.1 Barriers to large-scale deployment

CO_2 mineralization and storage involves the reaction of CO_2 with calcium- and magnesium-rich rocks and solid waste materials to produce stable carbonate minerals, such as calcite and dolomite. This process represents a significant technological pathway for achieving long-term and safe carbon sequestration (Lei et al., 2021; Rosenbauer et al., 2012; Wang et al., 2023). However, the technology encounters several challenges during large-scale engineering deployment. The suitability of geological storage is constrained by the need for spatial and temporal alignment between reservoir properties and engineering parameters (Goldberg and Slagle, 2009). Effective sequestration target areas must simultaneously fulfill multiple requirements, including mineral abundance, rock permeability, caprock integrity, and geothermal gradients. In global sedimentary basins, only approximately 7–12% contain sufficiently thick ultramafic formations, such as oceanic basalt and ophiolites, and their spatial distribution is highly uneven. For instance, basalt outcrops in regions like Iceland and Oman demonstrate high reactivity, with porosity values ranging from 12% to 25% (Noiriel and Soulaine, 2021).

Rock permeability serves as a critical limitation, as the permeability of basalt matrices is typically low and largely dependent on fracture networks for fluid pathways. Field measurements indicate that fracture permeability exhibits strong anisotropy, which can lead to fingering phenomena following CO_2 injection, resulting in local over-saturation in some areas while other regions remain inadequately reacted (Hellevang et al., 2013; Kumar and Shrivastava, 2019). Numerical simulations suggest that in typical basalt reservoirs, CO_2 injection rates exceeding 20 kg/s can cause carbonate precipitation that reduces permeability near the wellbore by 60% within six months. Therefore, pulse injection or acidizing may be neces-

sary to maintain long-term injectivity (Liu et al., 2019; Pham et al., 2014).

The deep geothermal gradient also significantly influences the mineralization pathway. When temperatures exceed 80°C, magnesite ($MgCO_3$) tends to form preferentially over hydromagnesite (McGrail et al., 2017). While magnesite is more stable, its high nucleation energy barrier can extend the induction period by 3 to 5 times. Additionally, fluid overpressure may activate faults; for example, the Wallula project in the United States observed a 20-fold increase in microseismic activity during injection, with a maximum magnitude of 2.3 (Wang et al., 2023). Furthermore, the presence of pyrite (FeS) in certain serpentinized peridotites can release hydrogen sulfide (H_2S) in acidic CO_2 fluids, posing corrosion risks to wellbore equipment and environmental toxicity concerns. The interplay of kinetic and geological constraints frequently results in actual sequestration efficiencies that fall short of laboratory predictions. For instance, field monitoring data from Iceland's CarbFix project indicate that while 95% of injected CO_2 mineralized within two years, the presence of clay interlayers has led to the establishment of sequestration "blind spots," allowing approximately 5% of CO_2 to migrate in a free state (Marieni et al., 2021).

Consequently, future technological development must establish a cross-scale cognitive framework that integrates molecular-scale reaction mechanisms with basin-scale transport patterns, thereby enhancing overall sequestration certainty through adaptive injection regulation.

7.2 Scientific and technical challenges

The large-scale deployment of CO_2 mineralization technology encounters multidimensional and multiscale scientific challenges, as well as technical challenges related to reaction kinetics. The reaction rate directly influences both the engineering feasibility and the scalability potential of this technological pathway (Ajoma et al., 2020). From the perspective of reaction kinetics, the dissolution-precipitation process of silicate minerals is constrained by intrinsic reaction rates, which are primarily governed by the dual limitations of molecular-scale interfacial reaction mechanisms and macroscopic mass transfer efficiencies (Gysi and Stefánsson, 2012; Wolff-Boenisch et al., 2004). The dissolution rates of silicate minerals, such as olivine and serpentine, are controlled by the stability of their crystal structures, resulting in relatively low dissolution rate constants under standard temperature and pressure conditions. This slow kinetic characteristic necessitates geological time scales for mineral carbonation to occur under natural conditions (Sigfússon et al., 2018).

Experimental studies demonstrate that the dissolution rate of minerals is highly sensitive to reaction conditions. For instance, increasing the temperature to 150–200°C can enhance the dissolution rate of olivine by 2 to 3 orders of magnitude, due to a reduction in activation energy from approximately 80 kJ/mol to around 50 kJ/mol (Phukan et al., 2021). An acidic environment (pH 3–5) can promote the leaching of magnesium ions via proton-driven mechanisms; however, excessive acidification (pH < 2) may result in the collapse of the silicate tetrahedral structure, subsequently inhibiting continuous reaction (Gislason et al., 2010). Moreover, the secondary minerals formed during the reaction, such as amorphous SiO_2 and layered double hydroxides, can develop dense passivation layers on the mineral surface. High-resolution transmission electron microscopy observations indicate that the thickness of these passivation layers can reach 50–200 nm, and their nanopore volume fraction (<10%) significantly obstructs the transport of reactants, leading to an exponential decay of the effective reactive surface area over time (Sun et al., 2022).

To address these limitations, current research efforts are focusing on synergistic activation strategies across multiple physical fields (Ali et al., 2019). In the domain of mechanochemistry, high-energy ball milling reduces the particle size of minerals to submicron levels, resulting not only in an increased specific surface area (from 0.5 to 5.3 m^2/g) but also in the introduction of dislocations and grain boundary defects within the particles, which can lower the dissolution activation energy by 30–40% (Waszczuk et al., 2016). In the field of catalytic chemistry, organic acid ligands (such as oxalic and citric acids) can selectively extract magnesium ions through chelation, leading to an increase in the dissolution rate of serpentine by 5 to 8 times. Additionally, biological enzymes (like carbonic anhydrase) can accelerate the generation of carbonate ions by lowering the hydration energy barrier of CO_2 (Hu et al., 2016). It is essential to note that although these enhancement methods have achieved significant breakthroughs at the laboratory scale, scaling them to industrial levels presents challenges related to energy consumption and costs. For example, maintaining a reaction temperature of 150°C necessitates continuous thermal energy input, resulting in an energy consumption of 1.2 to 1.8 GJ per ton of CO_2 sequestered, which substantially impacts the net reduction benefits of the entire process.

7.3 Engineering and operational hurdles

The integrity risks associated with wellbores in CO_2 geological storage present a complex challenge that encompasses multiple physicochemical processes. Central to this issue are the long-term interactions within the supercritical CO_2-brine-cement-steel multiphase system under conditions of high temperature and pressure. The wellbore system acts as the sole conduit linking the surface to the underground reservoir; consequently, any failure in its integrity may directly lead to sequestration failure, resource wastage, or even safety incidents (Lecolier et al., 2006; Li et al., 2015; Zhang et al., 2013).

From the standpoint of material degradation mechanisms, the carbonation process of the cement sheath exhibits distinct zonal characteristics. Following CO_2 infiltration in the near-wellbore region, a rapid carbonation reaction occurs, resulting in the transformation of $Ca(OH)_2$ and C-S-H gel into $CaCO_3$ and amorphous SiO_2. While this process initially enhances the density of the material, it can ultimately give rise to the formation of micro-annular gaps ranging from 10 to 50 μm at the cement-steel interface over time (Spokas et al., 2019). Notably, when the reservoir temperature exceeds 50°C, the rate of the carbonation reaction escalates exponentially. Accelerated testing has demonstrated that, under the influence of supercritical CO_2, the compressive strength of oilwell cement consistently

declines, while permeability exhibits an upward trend.

Furthermore, subsurface displacement resulting from reservoir compaction or uplift can induce shear deformation of the casing. This deformation may result in localized strains of up to 2% at the casing connections, which significantly surpasses the elastic limits of the steel (Zhang et al., 2013). From a monitoring perspective, the degradation of wellbore integrity often exhibits nonlinear characteristics. Data obtained from distributed fiber optic sensing indicate that early signs of damage to the cement sheath are manifested by a reduction in acoustic wave velocity and abnormal temperature gradients, while casing corrosion results in a systematic decrease in the rigidity of the pipe. However, once damage accumulates to a critical state, a sudden integrity failure can transpire within the system (Olsen and Rimstidt, 2008). Leakage resulting from well failure can lead to catastrophic incidents, as illustrated by a leakage event in a carbon sequestration project in Illinois.

This "gradual-then-sudden" behavior contributes to a high rate of false alarms in traditional threshold alarm systems, thereby underscoring the urgent necessity for the development of machine learning-based multi-parameter fusion early warning technologies. In terms of risk mitigation, the most effective current technological strategy involves the "material-structure-process" collaborative optimization aimed at reducing the carbonation rate. Additionally, the deployment of intelligent completion technologies can facilitate the automatic activation of sealing mechanisms upon the detection of micro-leaks. It is imperative to emphasize that the management of wellbore integrity must span the entire lifecycle of the sequestration project, encompassing rock mechanics evaluations during the drilling phase, real-time pressure control during the injection period, and long-term monitoring in the post-sequestration phase. Each stage of this process necessitates rigorous quality control and continuous technological innovation.

7.4 Economic and infrastructural barriers

The large-scale commercial application of CO_2 mineralization and storage technology confronts significant economic challenges. This cost is considerably higher than current carbon trading prices, which generally fall below $50 per ton (Hu et al., 2016).

From a technical perspective, the analysis of cost challenges reveals primary challenges across three stages: front-end raw material acquisition, mid-stage reaction intensification, and back-end product handling. In the front-end raw material supply chain, the costs associated with the mining and pretreatment of suitable silicate minerals for mineralization represent 35–45% of total expenses (Sjöberg and Rickard, 1985). Moreover, the geographical distribution of high-grade ore bodies is markedly uneven, with 90% of economically extractable reserves concentrated in a limited number of regions. This concentration results in elevated raw material costs due to long-distance transportation (Frisbee and Hossner, 1995).

Economic constraints in the mid-stage reaction intensification are even more pronounced. To address the limitations imposed by natural mineralization rates, existing technological pathways typically depend on high temperature, high pressure, or chemical additives (such as organic acids and ionic liquids) to enhance the process. However, these methods incur substantial operating costs (Wogelius and Walther, 1991). The thermal energy required to maintain continuous flow reactors at 200°C is estimated to be between 1.8 and 2.5 GJ per ton of CO_2, translating to fuel costs in the range of $30 to $45 per ton of CO_2 based on industrial natural gas prices (Al-Yaseri et al., 2021a). The often-overlooked hidden costs associated with back-end product disposal are significant, as each ton of mineralized CO_2 generates approximately 2.5 to 3.5 tons of solid waste. The management of these by-products requires seepage treatment or potential for value-added utilization, both of which are constrained by market capacity and transportation limitations (Ali et al., 2019).

It is important to recognize that cost variations may arise under different geological conditions. In-situ mineralization eliminates mineral extraction costs; however, the expenses related to drilling, completion, and monitoring requirements maintain high overall costs. Conversely, ex-situ mineralization, while enabling controlled reactions, encounters offsetting costs linked to CO_2 capture and transportation, thereby diminishing its technical advantages (Rimstidt et al., 2012). Evaluating the learning curve effect shows that the cost of mineralization technology has decreased by only 28% over the past decade, significantly lower than the cost reduction rates observed in photovoltaics and lithium batteries. This limitation is primarily due to the inherent complexity of the reaction processes, which hampers equipment standardization and the realization of economies of scale.

To overcome these economic challenges in the future, a multifaceted approach is essential. Developing low-grade mineral utilization technologies may contribute to lowering raw material costs (Phukan et al., 2021). Additionally, innovative catalytic systems, such as biomimetic carbonic anhydrases, show promise in moderating reaction conditions and reducing energy consumption by up to 60%. Furthermore, a CO_2-EOR collaborative model could facilitate shared infrastructure and shorten the return on investment period from 15 years to 8–10 years. Ultimately, the commercial-scale deployment of CO_2 mineralization and storage technologies is likely to materialize only when global carbon prices consistently exceed $80 per ton and when policies provide long-term guarantees of 10–15 years.

8 Conclusions

CO_2 mineralization has gained recognition as an effective carbon sequestration strategy owing to its inherent safety and long-term stability. This work presents a systematic review of recent progress in CO_2 mineralization technologies, with particular focus on three scenarios: (i) CO_2 mineralization in sandstones, (ii) in situ mineralization within basalt formations, and (iii) ex situ mineralization utilizing solid waste materials. Through an extensive analysis of representative studies across these three mineralization pathways, we critically evaluate recent technological advancements including: reaction acceleration methods, geothermal energy-enhanced mineralization processes, machine learning applications for mineralization process optimization, and advanced wellbore materials. The

review further identifies four critical challenges hindering the large-scale implementation of CO_2 mineralization for greenhouse gas mitigation: (1) Technical and logistical barriers to large-scale deployment; (2) Fundamental scientific challenges in reaction kinetics; (3) Potential leakage risks and long-term storage security; (4) Economic viability and cost-effectiveness considerations. Building upon this comprehensive assessment, we propose strategic research directions and potential solutions to address these challenges. This study provides both a timely synthesis of current knowledge and a framework to guide future research in CO_2 mineralization technologies.

Acknowledgements

The authors are grateful for the funding support provided by Open Fund of the State Key Laboratory of Intelligent Construction and Healthy Operation and Maintenance of Deep Underground Engineering (Project No. SDGZ2502), CNPC Innovation Fund (Project No. 2024DQ02-0141), and Chinese Academy of Sciences International Collaboration Project (Project No. 026GJHZ2024018MI).

Conflict of interest

The authors declare no competing interest.

References

Abdulelah H, Al-Yaseri A, Ali M, et al. 2021. CO_2/Basalt's interfacial tension and wettability directly from gas density: Implications for Carbon Geo-sequestration. *Journal of Petroleum Science and Engineering*, **204**: 108683. doi:10.1016/j.petrol.2021.108683.

Ajoma E, Saira, Sungkachart T, et al. 2020. Water-saturated CO_2 injection to improve oil recovery and CO_2 storage. *Applied Energy*, **266**: 114853. doi:10.1016/j.apenergy.2020.114853.

Al-Yaseri A, Ali M, Abbasi GR, et al. 2021. Enhancing CO_2 storage capacity and containment security of basaltic formation using silica nanofluids. *International Journal of Greenhouse Gas Control*, **112**: 103516. doi:10.1016/j.ijggc.2021.103516.

Al-Yaseri A, Ali M, Ali M, et al. 2021. Western Australia basalt-CO_2-brine wettability at geo-storage conditions. *Journal of Colloid and Interface Science*, **603**: 165–171. doi:10.1016/j.jcis.2021.06.078.

Ali M, Arif M, Sahito MF, et al. 2019. CO_2-wettability of sandstones exposed to traces of organic acids: Implications for CO_2 geo-storage. *International Journal of Greenhouse Gas Control*, **83**: 61–68. doi:10.1016/j.ijggc.2019.02.002.

Ali M, Yekeen N, Alanazi A, et al. 2023. Saudi Arabian basalt / CO_2 / brine wettability: Implications for CO_2. *Journal of Energy Storage*, **62**: 106921. doi: 10.1016/j.est.2023.106921.

Alkan H, Cinar Y, Ülker EB. 2010. Impact of capillary pressure, salinity and in situ conditions on CO_2 injection into saline aquifers. *Transport in Porous Media*. doi:10.1007/s11242-010-9541-8.

Aradóttir ESP, Sonnenthal EL, Jónsson H. 2012. Development and evaluation of a thermodynamic dataset for phases of interest in CO_2 mineral sequestration in basaltic rocks. *Chemical Geology*, **304–305**: 26–38. doi:10.1016/j.chemgeo.2012.01.031.

Arbad N, Emadi H, Watson M. 2022. A comprehensive review of geothermal cementing from well integrity perspective. *Journal of Petroleum Science and Engineering*, **217**: 110869. doi:10.1016/j.petrol.2022.110869.

Awad A, Koster Van Groos AF, Guggenheim S. 2000. Forsteritic olivine: Effect of crystallographic direction on dissolution kinetics. *Geochimica et Cosmochimica Acta*, **64**(10): 1765–1772. doi:10.1016/S0016-7037(99)00442-1.

Bandstra JZ, Brantley SL. 2008. Surface evolution of dissolving minerals investigated with a kinetic Ising model. *Geochimica et Cosmochimica Acta*, **72**(10): 2587–2600. doi:10.1016/j.gca.2008.02.023.

Bandstra JZ, Brantley SL. 2008. Data fitting techniques with applications to mineral dissolution kinetics. In: *Kinetics of Water-Rock Interaction*. p. 211–257. doi: 10.1007/978-0-387-73563-4_6.

Beaulieu E, Goddéris Y, Labat D, et al. 2010. Impact of atmospheric CO_2 levels on continental silicate weathering. *Geochemistry, Geophysics, Geosystems*, **11**. doi:10.1029/2010GC003078.

Beck J, Feng R, Hall DM, et al. 2016. Effects of H_2S and CO_2 on cement/casing interface corrosion integrity for cold climate oil and gas well applications. *ECS Transactions*, **72**(15): 107–122. doi:10.1149/ma2016-01/15/946.

Black JR, Carroll SA, Haese RR. 2015. Rates of mineral dissolution under CO_2 storage conditions. *Chemical Geology*, **399**: 134–144. doi:10.1016/j.chemgeo.2014.09.020.

Blum A, Lasaga A. 1988. Role of surface speciation in the low-temperature dissolution of minerals. *Nature*, **331**: 431-433. doi□10.1038/331431a0.

Borges E, Souza DP, Ulson De Souza AA, et al. 2007. Prediction of effective diffusivity tensors for bulk diffusion with chemical reactions in porous media. *Brazilian Journal of Chemical Engineering*. doi:10.1590/s0104-66322007000100005.

Cao X, Li Q, Xu L. 2023. A review of in situ carbon mineralization in basalt. *Journal of Rock Mechanics and Geotechnical Engineering*, **16**(4): 1–21. doi:10.1016/j.jrmge.2023.11.010.

Cao X, Li Q, Xu L, et al. 2024. Experiments of CO_2-basalt-fluid interactions and micromechanical alterations: implications for carbon mineralization. *Energy and Fuels*, **38**(9): 6205–6214. doi:10.1021/acs.energyfuels.4c00202.

Cárdenas-Escudero C, Morales-Flórez V, Pérez-López R, et al. 2011. Procedure to use phosphogypsum industrial waste for mineral CO_2 sequestration. *Journal of Hazardous Materials*, **196**: 431–435. doi:10.1016/j.jhazmat.2011.09.039.

Carroll SA, Knauss KG. 2005. Dependence of labradorite dissolution kinetics on CO_2(aq), Al(aq), and temperature. *Chemical Geology*, **217**(3-4): 213–225. doi:10.1016/j.chemgeo.2004.12.008.

Cecen A, Dai H, Yabansu YC, et al. 2018. Material structure-property linkages using three-dimensional convolutional neural networks. *Acta Materialia*. **146**: 76–84. doi:10.1016/j.actamat.7.11.053.

Chaïrat C, Schott J, Oelkers EH, et al. 2007. Kinetics and mechanism of natural fluorapatite dissolution at 25°C and pH from 3 to 12. *Geochimica et Cosmochimica Acta*, **71**(24): 5901–5912. doi:10.1016/j.gca.2007.08.031.

Chen Z, Cang Z, Yang F, et al. 2021. Carbonation of steelmaking slag presents an opportunity for carbon neu-

tral: A review. *Journal of CO_2 Utilization*, **54**: 101738. doi:10.1016/j.jcou.2021.101738.

Choubineh A, Helalizadeh A, Wood D A. 2019. Estimation of minimum miscibility pressure of varied gas compositions and reservoir crude oil over a wide range of conditions using an artificial neural network model. *Advances in Geo-Energy Research*, **3**(1): 52–66. doi:10.26804/ager.2019.01.04.

Deng H, Gharasoo M, Zhang L, et al. 2022. A perspective on applied geochemistry in porous media: Reactive transport modeling of geochemical dynamics and the interplay with flow phenomena and physical alteration. *Applied Geochemistry*, **146**: 105445. doi:10.1016/j.apgeochem.2022.105445.

Dessert C, Dupré B, Gaillardet J, et al. 2003. Basalt weathering laws and the impact of basalt weathering on the global carbon cycle. *Chemical Geology*, **202**(3-4): 257–273. doi:10.1016/j.chemgeo.2002.10.001.

Duan D, Song H, Wei F, et al. 2024. Mechanical properties of solid waste-based composite cementitious system enhanced by CO_2 modification. *Construction and Building Materials*, **426**: 136187. doi:10.1016/j.conbuildmat.2024.136187.

Ebrahimi A, Saffari M, Hong Y, et al. 2018. Mineral sequestration of CO_2 using saprolite mine tailings in the presence of alkaline industrial wastes. *Journal of Cleaner Production*, **188**: 686–697. doi:10.1016/j.jclepro.2018.04.046.

Ebrahimi A, Saffari M, Milani D, et al. 2017. Sustainable transformation of fly ash industrial waste into a construction cement blend via CO_2 carbonation. *Journal of Cleaner Production*, **156**: 660–669. doi:10.1016/j.jclepro.2017.04.037.

Edouard MN, Okere CJ, Ejike C, et al. 2023. Comparative numerical study on the co-optimization of CO_2 storage and utilization in EOR, EGR, and EWR: Implications for C-CUS project development. *Applied Energy*, **347**: 121448. doi:10.1016/j.apenergy.2023.121448.

Ennis-King J, Paterson L. 2007. Coupling of geochemical reactions and convective mixing in the long-term geological storage of carbon dioxide. *International Journal of Greenhouse Gas Control*, **1**(1): 86–93. doi:10.1016/S1750-5836(07)00034-5.

Flaathen TK, Gislason SR, Oelkers EH. 2010. The effect of aqueous sulphate on basaltic glass dissolution rates. *Chemical Geology*, **277**(3-4): 345–354. doi:10.1016/j.chemgeo.2010.08.018.

Frisbee NM, Hossner LR. 1995. Siderite Weathering in Acidic Solutions under Carbon Dioxide, Air, and Oxygen. *Journal of Environmental Quality*, **24**(5): 856–860. doi: 10.2134/jeq1995.00472425002400050010x.

Gan M, Zhang L, Miao X, et al. 2020. Application of computed tomography (CT) in geologic CO_2 utilization and storage research: A critical review. *Journal of Natural Gas Science and Engineering*, **83**: 103591. doi:10.1016/j.jngse.2020.103591.

Gan M, Zhang L, Wang Y, et al. 2025. Discovery of a surge in alteration depth of wellbore cement exposed to high concentration CO_2 from 28 days to 56 days. *Geoenergy Science and Engineering*, **253**: 213970. doi:10.1016/j.geoen.2025.213970.

Gautier JM, Oelkers EH, Schott J. 2001. Are quartz dissolution rates proportional to B.E.T. surface areas? *Geochimica et Cosmochimica Acta*, **65**(7): 1059–1070. doi:10.1016/S0016-7037(00)00570-6.

Geloni C, Giorgis T, Battistelli A. 2011. Modeling of Rocks and Cement Alteration due to CO_2 Injection in an Exploited Gas Reservoir. *Transport in Porous Media*, **90**(1): 183–200. doi:10.1007/s11242-011-9714-0.

Ghanbarian B, Hunt AG. 2017. Fractals: Concepts and applications in geosciences. *Fractals: Concepts and Applications in Geosciences*. doi:10.1201/9781315152264.

Giammar DE, Bruant RG, Peters CA. 2005. Forsterite dissolution and magnesite precipitation at conditions relevant for deep saline aquifer storage and sequestration of carbon dioxide. *Chemical Geology*, **217**(3-4): 257–276. doi:10.1016/j.chemgeo.2004.12.013.

Gislason SR, Oelkers EH. 2003. Mechanism, rates, and consequences of basaltic glass dissolution: II. An experimental study of the dissolution rates of basaltic glass as a function of pH and temperature. *Geochimica et Cosmochimica Acta*, **67**(20): 3817–3832. doi:10.1016/S0016-7037(00)00176-5.

Gíslason SR, Sigurdardóttir H, Aradóttir ES, et al. 2018. A brief history of CarbFix: Challenges and victories of the project's pilot phase. *Energy Procedia*, **146**: 103–114. doi:10.1016/j.egypro.2018.07.014.

Gislason S R, Wolff-Boenisch D, Stefansson A, et al. 2010. Mineral sequestration of carbon dioxide in basalt: A preinjection overview of the CarbFix project. *International Journal of Greenhouse Gas Control*, **4**(3): 537–545. doi:10.1016/j.ijggc.2009.11.013.

Goldberg D, Slagle AL. 2009. A global assessment of deep-sea basalt sites for carbon sequestration. *Energy Procedia*, **1**(1): 3675–3682. doi:10.1016/j.egypro.2009.02.165.

Golubev SV, Pokrovsky OS, Schott J. 2005. Experimental determination of the effect of dissolved CO_2 on the dissolution kinetics of Mg and Ca silicates at 25 °C. *Chemical Geology*, **217**(3-4): 227–238. doi:10.1016/j.chemgeo.2004.12.011.

Grandstaff DE. 1978. Changes in surface area and morphology and the mechanism of forsterite dissolution. *Geochimica et Cosmochimica Acta*, **42**(12): 1899–1901. doi:10.1016/0016-7037(78)90245-4.

Grünhäuser Soares E, Castro-Gomes J, Sitarz M, et al. 2022. Feasibility for co-utilisation of Carbonated Reactive Magnesia Cement (CRMC) and industrial wastes in circular economy and CO_2 mineralisation. *Construction and Building Materials*, **323**: 126488. doi:10.1016/j.conbuildmat.2022.126488.

Gudbrandsson S, Wolff-Boenisch D, Gislason SR, et al. 2014. Experimental determination of plagioclase dissolution rates as a function of its composition and pH at 22°C. *Geochimica et Cosmochimica Acta*, **139**: 154–172. doi:10.1016/j.gca.2014.04.028.

Gudbrandsson S, Wolff-Boenisch D, Gíslason SR, et al. 2008. Dissolution rates of crystalline basalt at pH 4 and 10 and 25-75°C. *Mineralogical Magazine*, **72**(1): 155–158. doi:10.1180/minmag.2008.072.1.155.

Gunter WD, Perkins E, McCann TJ. 1993. Aquifer disposal of CO_2-rich gases: Reaction design for added capacity. *Energy Conversion and Management*, **34**(9-11): 941–948. doi:10.1016/0196-8904(93)90040-H.

Gysi AP, Stefánsson A. 2012. CO_2-water-basalt interaction. Low temperature experiments and implications for CO_2 sequestration into basalts. *Geochimica et Cosmochimica Acta*, **81**: 129–152. doi:10.1016/j.gca.2012.01.012.

Han G, Han WS, Kim KY, et al. 2019. Roles of fault structures and regional formations on CO_2 migration and distribution in shallow saline aquifer in Green River, Utah. *Journal of Hydrology*, **570**: 786–801. doi:10.1016/j.jhydrol.2019.01.027.

Hänchen M, Prigiobbe V, Storti G, et al. 2006. Dissolution kinetics of fosteritic olivine at 90-150 °C including effects of the presence of CO_2. *Geochimica et Cosmochimica Acta*, **70**(17): 4403–4416. doi:10.1016/j.gca.2006.06.1560.

Hellevang H, Pham VTH, Aagaard P. 2013. Kinetic modelling of CO_2-water-rock interactions. *International Journal of Greenhouse Gas Control*, **15**: 3–15.

doi:10.1016/j.ijggc.3.01.027.
Hu Y, Liu W, Sun J, et al. 2016. Structurally improved CaO-based sorbent by organic acids for high temperature CO_2 capture. *Fuel*, **167**: 17–24. doi:10.1016/j.fuel.2015.11.048.
Iglauer S, Al-Yaseri A. 2021. Improving basalt wettability to de-risk CO_2 geo-storage in basaltic formations. *Advances in Geo-Energy Research*, **5**(3): 347–350. doi:10.46690/AGER.2021.03.09.
Intergovernmental Panel on Climate Change (IPCC). 2022. Global warming of 1.5°C: IPCC special report on impacts of global warming of 1.5°C above pre-industrial levels in scenario of strengthening response to climate change, sustainable development, and efforts to eradicate poverty. Cambridge University Press, Cambridge. doi:10.1017/9781009157940.
IPCC. 2023. AR6 Synthesis Report: Climate Change 2023. Cambridge. https://www.ipcc.ch/report/sixth-assessment-report-cycle/.
Izgec O, Demiral B, Bertin H, et al. 2008. CO_2 injection into saline carbonate aquifer formations II: Comparison of numerical simulations to experiments. *Transport in Porous Media*. doi:10.1007/s11242-007-9160-1.
Jacquemet N, Pironon J, Lagneau V, et al. 2012. Armouring of well cement in H_2S-CO_2 saturated brine by calcite coating - Experiments and numerical modelling. *Applied Geochemistry*, **27**(4): 782–795. doi:10.1016/j.apgeochem.2011.12.004.
Jang K, Moulay I, Lee D, et al. 2025. Sustainable conversion of oyster shell waste into high-purity calcium carbonate via CO_2 mineralization. *Journal of Environmental Chemical Engineering*, **13**(1): 115099. doi:10.1016/j.jece.2024.115099.
Jarvis K, Carpenter RW, Windman T, et al. 2009. Reaction mechanisms for enhancing mineral sequestration of CO_2. *Environmental Science & Technology*, **43**(16): 6314–6319. doi:10.1021/es8033507.
Jeschke AA, Dreybrodt W. 2002. Dissolution rates of minerals and their relation to surface morphology. *Geochimica et Cosmochimica Acta*, **66**(17): 3055–3062. doi:10.1016/S0016-7037(02)00893-1.
Johnson JW, Nitao JJ, Morris JP. 2005. Reactive transport modeling of cap-rock integrity during natural and engineered CO_2 storage. In: *Carbon Dioxide Capture for Storage in Deep Geologic Formations - Results from the CO_2 Capture Project*. p. 787–813. doi:10.1016/B978-008044570-0/50134-3.
Johnson K. 1992. Regulation update - clean water & phosphogypsum. *Proceedings of the 42nd Annual Meeting - Fertilizer Industry Round Table*: 1992.
Kaithwas A, Prasad M, Kulshreshtha A, et al. 2012. Industrial wastes derived solid adsorbents for CO_2 capture: A mini review. *Chemical Engineering Research and Design*, **90**(10): 1632–1641. doi:10.1016/j.cherd.2012.02.011.
Kammerer S, Borho I, Jung J, et al. 2023. Review: CO_2 capturing methods of the last two decades. *International Journal of Environmental Science and Technology*, **20**(7): 8087–8104. doi:10.1007/s13762-022-04680-0.
Kampman N, Bickle M, Becker J, et al. 2009. Feldspar dissolution kinetics and Gibbs free energy dependence in a CO_2-enriched groundwater system, Green River, Utah. *Earth and Planetary Science Letters*, **284**(3-4): 473–488. doi:10.1016/j.epsl.2009.05.013.
Kaptan K, Cunha S, Aguiar J. 2024. A Review: Construction and Demolition Waste as a Novel Source for CO_2 Reduction in Portland Cement Production for Concrete. *Sustainability*, **16**(2): 585. doi:10.3390/su16020585.
Karishma S, Kamalesh R, Saravanan A, et al. 2024. A review on recent advancements in biochemical fixation and transformation of CO_2 into constructive products. *Biochemical Engineering Journal*, **208**: 109366. doi:10.1016/j.bej.2024.109366.
Knauss KG, Johnson JW, Steefel CI. 2005. CO_2 sequestration in the Frio Fm., TX: Evaluation of the impact of CO_2, co-contaminant gas, aqueous fluid and reservoir rock interactions. In: *Second Annual Conference on Carbon Sequestration*.
Kravchenko E, Sauerwein M, Besklubova S, et al. 2024. A comparative life cycle assessment of recycling waste concrete powder into CO_2-Capture products. *Journal of Environmental Management*, **352**: 119947. doi:10.1016/j.jenvman.2023.119947.
Kresge CT, Roth WJ, Vartuli JC, et al. 1992. Control of dissolution rates of orthosilicate minerals by divalent metal-oxygen bonds. *Nature*, **355**: 157-159. doi:10.1038/355157a0.
Kumar A, Shrivastava JP. 2019. Carbon capture induced changes in Deccan basalt: a mass-balance approach. *Greenhouse Gases: Science and Technology*, **9**(6): 1158–1180. doi:10.1002/ghg.1923.
Kump LR, Brantley SL, Arthur MA. 2000. Chemical weathering, atmospheric CO_2 and climate. *Annual Review of Earth and Planetary Sciences*, **28**: 611–667. doi: 10.1146/annurev.earth.28.1.611.
Kuoribo E, Shokry H, Mahmoud H. 2024. Attaining material circularity in recycled construction waste to produce sustainable concrete blocks for residential building applications. *Journal of Building Engineering*, **96**: 110503. doi:10.1016/j.jobe.2024.110503.
Kusin FM, Syed Hasan SNM, Molahid VLM, et al. 2024. Dual adoption opportunities and prospects for mining and industrial waste recovery through an integrated carbon capture, utilization and storage. *Sustainable Production and Consumption*, **48**: 181–204. doi:10.1016/j.spc.2024.05.012.
Kutchko BG, Lopano CL, Strazisar BR, et al. 2015. Impact of oil well cement exposed to H_2S saturated fluid and gas at high temperatures and pressures: implications for acid gas injection and co-sequestration. *Journal of Sustainable Energy Engineering*, **3**(1): 80–101. doi:10.7569/jsee.2015.629509.
Lasaga AC. 1984. Chemical kinetics of water-rock interactions. *Geochimica et Cosmochimica Acta*, **48**(7): 4009–4025. doi:10.1029/JB089iB06p04009.
Lecolier E, Rivereau A, Ferrer N, et al. 2006. Durability of oilwell cement formulations aged in H_2S-containing fluids. *Proceedings of the IADC/SPE Drilling Conference*. **25**(01):90-95. doi:10.2118/99105-PA.
Lee RP, Seidl LG, Huang Q, et al. 2021. An analysis of waste gasification and its contribution to China's transition towards carbon neutrality and zero waste cities. *Journal of Fuel Chemistry and Technology*, **49**(8): 1057–1076. doi:10.1016/S1872-5813(21)60093-2.
Lehmann J, Possinger A. 2020. Atmospheric CO_2 removed by rock weathering. *Nature*, **583**(7815): 204–205. doi:10.1038/d41586-020-01965-7.
Lei Z, Zhang Y, Zhou L, et al. 2021. Numerical simulation of CO_2 mineral sequestration in basalt reservoir through an abandoned oil well: a case study in Xujiaweizi area, Northeast China. *Environmental Earth Sciences*, **80**(3): 1–22. doi:10.1007/s12665-021-09876-0.
Li Z, Chen J, Lv Z, et al. 2023. Evaluation on direct aqueous carbonation of industrial/mining solid wastes for CO_2 mineralization. *Journal of Industrial and Engineering Chemistry*, **122**: 359–365. doi:10.1016/j.jiec.2023.02.036.
Li Z, Gu T, Guo X, et al. 2015. Characterization of the unidi-

rectional corrosion of oilwell cement exposed to H_2S under high-sulfur gas reservoir conditions. *RSC Advances*, **5**(87): 71529–71536. doi:10.1039/c5ra12481f.

Lin Z, Liu K, Liu J, et al. 2021. Numerical model for geothermal energy utilization from double pipe heat exchanger in abandoned oil wells. *Advances in Geo-Energy Research*, **5**(2): 212–221. doi:10.46690/ager.2021.02.10.

Tian LN. 2002. Comprehensive Utilization of Phosphogypsum. *Chemical Industry and Engineering Progress*. **21**(1):56-59.

Lindeberg E, Wessel-Berg D. 1997. Vertical convection in an aquifer column under a gas cap of CO_2. *Energy Conversion and Management*, **38**: S229–S234. doi:10.1016/S0196-8904(96)00274-9.

Liu D, Agarwal R, Li Y, et al. 2019. Reactive transport modeling of mineral carbonation in unaltered and altered basalts during CO_2 sequestration. *International Journal of Greenhouse Gas Control*, **85**: 109–120. doi:10.1016/j.ijggc.2019.04.006.

Liu J, Cheng L, Jin H, et al. 2024. Sustainable utilization of concrete slurry waste in eco-friendly artificial lightweight cold-bonded aggregates: An alternative pathway for efficiently sequestrating CO_2. *Construction and Building Materials*, **421**: 135759. doi:10.1016/j.conbuildmat.2024.135759.

Liu W, Teng L, Rohani S, et al. 2021. CO_2 mineral carbonation using industrial solid wastes: A review of recent developments. *Chemical Engineering Journal*, **416**: 129093. doi:10.1016/j.cej.2021.129093.

Liu Z, Luo S, Liu S, et al. 2025. Revealing the underlying mechanism behind CO_2 curing light porous solid-waste based concrete. *Construction and Building Materials*, **465**: 140129. doi:10.1016/j.conbuildmat.2025.140129.

Loubser MJ. 2013. Weathering of basalt and sandstone by wetting and drying: A process isolation study. *Geografiska Annaler: Series A, Physical Geography*, **95**(4): 295–304. doi:10.1111/geoa.12023.

Luan C, Zhou A, Li Y, et al. 2024. CO_2 avoidance cost of fly ash geopolymer concrete. *Construction and Building Materials*, **416**: 135193. doi:10.1016/j.conbuildmat.2024.135193.

Luhmann AJ, Tutolo BM, Bagley BC, et al. 2017. Permeability, porosity, and mineral surface area changes in basalt cores induced by reactive transport of CO_2-rich brine. *Water Resources Research*, **53**(3): 1908–1927. doi:10.1002/2016WR019216.

Luo S, Gao S, Yang L, et al. 2024. Enhancing coal gangue aggregates with fly ash-cement slurry: Synergistic effects of CO_2 mineralization on physical and mechanical properties. *Construction and Building Materials*, **440**: 137389. doi:10.1016/j.conbuildmat.2024.137389.

Maher K, Chamberlain C. 2014. Hydrologic regulation of chemical weathering and the geologic carbon cycle. *Science*,**343**,(6178):1502-1504. doi:10.1126/science.125077.

Marieni C, Voigt M, Clark DE, et al. 2021. Mineralization potential of water-dissolved CO_2 and H_2S injected into basalts as function of temperature: Freshwater versus Seawater. *International Journal of Greenhouse Gas Control*, **109**: 103357. doi:10.1016/j.ijggc.2021.103357.

Matter JM, Broecker WS, Gislason SR, et al. 2011. The CarbFix Pilot Project - Storing carbon dioxide in basalt. *Energy Procedia*, **4**: 5579–5585. doi:10.1016/j.egypro.2011.02.546.

Mayerich D, Sun R, Guo J. 2022. Deep Learning. In: *Microscope Image Processing, Second Edition*. p. 437–456. doi:10.1016/B978-0-12-821049-9.00015-0.

Mcgrail B, Ho A, Reidel S, et al. 2003. Use and features of basalt formations for geologic sequestration. *Greenhouse Gas Control Technologies - 6th International Conference*, **2**: 1637–1640. doi:10.1016/b978-008044276-1/50264-6.

McGrail BP, Schaef HT, Spane FA, et al. 2017. Field validation of supercritical CO_2 reactivity with basalts. *Environmental Science & Technology Letters*, **4**(1): 6–10. doi:10.1021/acs.estlett.6b00387.

Metz V, Amram K, Ganor J. 2005. Stoichiometry of smectite dissolution reaction. *Geochimica et Cosmochimica Acta*, **69**(7): 1755–1772. doi:10.1016/j.gca.2004.09.027.

Miocic JM, Johnson G, Gilfillan SMV. 2014. Fault seal analysis of a natural CO_2 reservoir in the Southern North Sea. *Energy Procedia*, **63**: 3364–3370. doi:10.1016/j.egypro.2014.11.365.

Moore J, Lichtner PC, White AF, et al. 2012. Using a reactive transport model to elucidate differences between laboratory and field dissolution rates in regolith. *Geochimica et Cosmochimica Acta*. doi:10.1016/j.gca.2012.03.021.

Moosdorf N, Renforth P, Hartmann J. 2014. Carbon dioxide efficiency of terrestrial enhanced weathering. *Environmental Science & Technology*, **48**(9): 4809–4816. doi:10.1021/es4052022.

Morales-Flórez V, Santos A, Lemus A, et al. 2011. Artificial weathering pools of calcium-rich industrial waste for CO_2 sequestration. *Chemical Engineering Journal*, **166**(1): 132–137. doi:10.1016/j.cej.2010.10.039.

Morrow CP, Kubicki JD, Mueller KT, et al. 2010. Description of Mg^{2+} release from forsterite using ab initio methods. *The Journal of Physical Chemistry C*, **114**(12): 5417–5428. doi:10.1021/jp9057719.

Morse JW, Arvidson RS. 2002. The dissolution kinetics of major sedimentary carbonate minerals. *Earth-Science Reviews*, **58**(1-2): 51–84. doi:10.1016/S0012-8252(01)00083-6.

Munz IA, Brandvoll Ø, Haug TA, et al. 2012. Mechanisms and rates of plagioclase carbonation reactions. *Geochimica et Cosmochimica Acta*, **77**: 27–51. doi:10.1016/j.gca.2011.10.036.

Naguib HM. 2024. CO_2 capture and storage in solid waste and low-carbon reactants for sustainable construction composites. *Egyptian Journal of Chemistry*, **67**(2): 439–450. doi:10.21608/EJCHEM.2024.260742.9150.

Nakao A, Morlando D, Knuutila HK. 2025. Techno-economic assessment of the multi-absorber approach at an industrial site with multiple CO_2 sources. *International Journal of Greenhouse Gas Control*, **142**: 104326. doi:10.1016/j.ijggc.2025.104326.

Navarro Á, Fonts I, Ruiz J, et al. 2025. The role of biogenic waste composition on pyrolysis: Part II – Char CO_2 adsorption capacity. *Biomass and Bioenergy*, **197**: 107775. doi:10.1016/j.biombioe.2025.107775.

Niu Y, Li T, Barzagli F, et al. 2024. Fly ash as a cost-effective catalyst to promote sorbent regeneration for energy efficient CO_2 capture. *Energy*, **294**: 130890. doi:10.1016/j.energy.2024.130890.

Noack Y, Colin F, Nahon D, et al. 1993. Secondary-mineral formation during natural weathering of pyroxene; review and thermodynamic approach. *American Journal of Science*, **293**(2): 111–134. doi: 10.2475/ajs.293.2.111.

Noiriel C, Soulaine C. 2021. Pore-scale imaging and modelling of reactive flow in evolving porous media: tracking the dynamics of the fluid-rock interface. *Transport in Porous Media*, **138**(1): 1–30. doi:10.1007/s11242-021-01613-2.

Oelkers EH. 2001. An experimental study of forsterite dissolution rates as a function of temperature and aqueous Mg and Si concentrations. *Chemical Geology*, **175**(3-4): 485–494. doi:10.1016/S0009-2541(00)00352-1.

Oelkers EH, Butcher R, Pogge von Strandmann PAE, et

al. 2019. Using stable Mg isotope signatures to assess the fate of magnesium during the in situ mineralisation of CO_2 and H_2S at the CarbFix site in SW-Iceland. *Geochimica et Cosmochimica Acta*, **245**: 542–555. doi:10.1016/j.gca.2018.11.011.

Oelkers EH, Cole DR. 2008. Carbon dioxide sequestration: A solution to a global problem. *Elements*, **4**(5): 305–310. doi:10.2113/gselements.4.5.305.

Oelkers EH, Gislason SR. 2001. The mechanism, rates and consequences of basaltic glass dissolution: I. An experimental study of the dissolution rates of basaltic glass as a function of aqueous Al, Si and oxalic acid concentration at 25°C and pH = 3 and 11. *Geochimica et Cosmochimica Acta*, **65**(21): 3671–3681. doi: 10.1016/S0016-7037(01)00664-0.

Olsen AA, Donald Rimstidt J. 2008. Oxalate-promoted forsterite dissolution at low pH. *Geochimica et Cosmochimica Acta*, **72**(7): 1758–1766. doi:10.1016/j.gca.2007.12.026.

Peng J, Xia B. 2024. Multi-field and multi-scale dynamic numerical modeling of supercritical CO_2 and fly ash mineralization. *Applied Thermal Engineering*, **257**: 124195. doi:10.1016/j.applthermaleng.2024.124195.

Pham THV, Aagaard P, Hellevang H. 2014. On the potential for CO_2 mineral storage in continental flood basalts-phreeqc batch and 1d diffusion-reaction simulations. In: *Carbon Capture Storage CO_2 Management Technol*. p. 178–202. doi:10.1201/b16845.

Phukan M, Vu HP, Haese RR. 2021. Mineral dissolution and precipitation reactions and their net balance controlled by mineral surface area: An experimental study on the interactions between continental flood basalts and CO_2-saturated water at 80 bars and 60 °C. *Chemical Geology*, **559**: 119909. doi:10.1016/j.chemgeo.2020.119909.

Pogge von Strandmann PAE, Burton KW, Snæbjörnsdóttir SO, et al. 2019. Rapid CO_2 mineralisation into calcite at the CarbFix storage site quantified using calcium isotopes. *Nature Communications*, **10**(1): 1–8. doi:10.1038/s41467-019-10003-8.

Prigiobbe V, Costa G, Baciocchi R, et al. 2009. The effect of CO_2 and salinity on olivine dissolution kinetics at 120 °C. *Chemical Engineering Science*, **64**(14): 3510–3515. doi:10.1016/j.ces.2009.04.035.

Raganati F, Miccio F, Iervolino G, et al. 2024. Waste-derived tuff for CO_2 Capture: Enhanced CO_2 adsorption performances by Cation-Exchange tailoring. *Journal of Industrial and Engineering Chemistry*, **138**: 153–164. doi:10.1016/j.jiec.2024.03.049.

Rahman MJ, Fawad M, Chan Choi J, et al. 2022. Effect of overburden spatial variability on field-scale geomechanical modeling of potential CO_2 storage site Smeaheia, offshore Norway. *Journal of Natural Gas Science and Engineering*, **99**: 104453. doi:10.1016/j.jngse.2022.104453.

Rahmani O. 2020. An experimental study of accelerated mineral carbonation of industrial waste red gypsum for CO_2 sequestration. *Journal of CO_2 Utilization*, **35**: 265–271. doi:10.1016/j.jcou.2019.10.005.

Rahmani O. 2018. CO_2 sequestration by indirect mineral carbonation of industrial waste red gypsum. *Journal of CO_2 Utilization*, **27**: 374–380. doi:10.1016/j.jcou.2018.08.017.

Ramasenya K, Oladipo B, Katambwe VN, et al. 2025. Comparative study of direct and indirect aqueous mineral carbonation of construction and demolition waste fines for CO_2 sequestration. *Journal of Environmental Chemical Engineering*, **13**(1): 117754. doi:10.1016/j.jece.2025.117754.

Rani N, Pathak V, Shrivastava JP. 2013. CO_2 mineral trapping: an experimental study on the carbonation of basalts from the eastern Deccan Volcanic. *Procedia Earth and Planetary Science*, **7**: 806–809. doi:10.1016/j.proeps.2013.03.069.

Ravichandran P, Rampradheep GS, Jagan S. 2024. Sustainable treatment approach to dumped construction waste with acids and CO_2 for its effective re-utilization in concrete. *Global NEST Journal*, **26**. doi:10.30955/gnj.005540.

Ren C, Wang W, Yao Y, et al. 2020. Complementary use of industrial solid wastes to produce green materials and their role in CO_2 reduction. *Journal of Cleaner Production*, **252**: 119840. doi:10.1016/j.jclepro.2019.119840.

Rimstidt JD, Brantley SL, Olsen AA. 2012. Systematic review of forsterite dissolution rate data. *Geochimica et Cosmochimica Acta*, **99**: 159–178. doi:10.1016/j.gca.2012.09.019.

Rosenbauer RJ, Thomas B, Bischoff JL, et al. 2012. Carbon sequestration via reaction with basaltic rocks: Geochemical modeling and experimental results. *Geochimica et Cosmochimica Acta*, **89**: 116–133. doi:10.1016/j.gca.2012.04.042.

Rosso JJ, Rimstidt JD. 2000. A high resolution study of forsterite dissolution rates. *Geochimica et Cosmochimica Acta*, **64**(5): 797–811. doi:10.1016/S0016-7037(99)00354-3.

Sahimi M, Hashemi M. 2001. Wavelet identification of the spatial distribution of fractures. *Geophysical Research Letters*, **28**(4): 611–614. doi:10.1029/2000GL011961.

Schaef HT, McGrail BP, Owen AT. 2011. Basalt reactivity variability with reservoir depth in supercritical CO_2 and aqueous phases. *Energy Procedia*, **4**: 4977–4984. doi:10.1016/j.egypro.1.02.468.

Schwartz MO. 2022. Can CO_2 sequestration in basalt efficiently reduce greenhouse gas emission? *Environmental Technology*, **43**(8): 1082–1092. doi:10.1080/09593330.2020.1815859.

Schwartz MO. 2018. Le nouveau projet Wallula CO_2 pourrait relancer l'ancien projet de stockage de déchets nucléaires dans les basaltes de la Columbia River (ouest des Etats-Unis d'Amérique). *Hydrogeology Journal*, **26**(1): 3–6. doi:10.1007/s10040-017-1632-y.

Senthilkumar AK, Kumar M, Kader MA, et al. 2025. Unveiling the CO_2 adsorption capabilities of carbon nanostructures from biomass waste: An extensive review. *Carbon Capture Science & Technology*, **14**: 100339. doi:10.1016/j.ccst.2024.100339.

Seyama H, Soma M, Tanaka A. 1996. Surface characterization of acid-leached olivines by X-ray photoelectron spectroscopy. *Chemical Geology*, **129**(3-4): 209–216. doi:10.1016/0009-2541(95)00142-5.

Siegel DI, Pfannkuch HO. 1984. Silicate mineral dissolution at pH 4 and near standard temperature and pressure. *Geochimica et Cosmochimica Acta*, **48**(2): 197–201. doi:10.1016/0016-7037(84)90362-4.

Sigfússon B, Arnarson MP, Snæbjörnsdóttir SÓ, et al. 2018. Reducing emissions of carbon dioxide and hydrogen sulphide at Hellisheidi power plant in 2014-2017 and the role of CarbFix in achieving the 2040 Iceland climate goals. *Energy Procedia*, **146**: 135–145. doi:10.1016/j.egypro.2018.07.018.

Singh S, Maiti S, Bisht RS, et al. 2024. Large CO_2 reduction and enhanced thermal performance of agro-forestry, construction and demolition waste based fly ash bricks for sustainable construction. *Scientific Reports*, **14**(1): 1–15. doi:10.1038/s41598-024-59012-8.

Sjöberg EL, Rickard DT. 1985. The effect of added dissolved calcium on calcite dissolution kinetics in aqueous solutions at 25°C. *Chemical Geology*, **49**(1-3): 405–413. doi:10.1016/0009-2541(85)90002-6.

Snæbjörnsdóttir S, Oelkers EH, Mesfin K, et al. 2017. The

chemistry and saturation states of subsurface fluids during the in situ mineralisation of CO2 and H2S at the CarbFix site in SW-Iceland. *International Journal of Greenhouse Gas Control*, **58**: 87–102. doi:10.1016/j.ijggc.2017.01.007.

Snæbjörnsdóttir S, Sigfússon B, Marieni C, et al. 2020. Carbon dioxide storage through mineral carbonation. *Nature Reviews Earth & Environment*, **1**(2): 90–102. doi:10.1038/s43017-019-0011-8.

Song R, Wu MY, Liu JJ, et al. 2024. Pore scale modeling on microbial hydrogen consumption and mass transfer of multicomponent gas flow in underground hydrogen storage of depleted reservoir. *Energy*, **306**: 132534. doi:10.1016/j.energy.2024.132534.

Song R, Wu MY, Wang Y, et al. 2023. In-situ X-CT scanning and numerical modeling on the mechanical behavior of the 3D printing rock. *Powder Technology*, **416**: 118240. doi:10.1016/j.powtec.2023.118240.

Spokas K, Fang Y, Fitts JP, et al. 2019. Collapse of Reacted Fracture Surface Decreases Permeability and Frictional Strength. *Journal of Geophysical Research: Solid Earth*, **124**(12): 12799–12811. doi:10.1029/2019JB017805.

Squires K, Wolf GH. 2006. Carbon sequestration via aqueous olivine mineral carbonation: role of passivating layer formation. *Environmental Science & Technology*, **40**(15): 4802–4808. doi:10.1021/es0523340.

Sun S, Zheng X, Liu X, et al. 2022. Global pattern and drivers of water scarcity research: a combined bibliometric and geographic detector study. *Environmental Monitoring and Assessment*, **194**(10). doi:10.1007/s10661-022-10142-4.

Szczygiel I, Jagoda Z. 2013. Phosphogypsum. The possibilities of the use. *Przemysl Chemiczny*, **92**(6): 970–974.

Tayari F, Blumsack S. 2020. A real options approach to production and injection timing under uncertainty for CO_2 sequestration in depleted shale gas reservoirs. *Applied Energy*, **263**: 114491. doi:10.1016/j.apenergy.2020.114491.

Tempel RN, Harrison WJ. 2000. Simulation of burial diagenesis in the Eocene Wilcox Group of the Gulf of Mexico basin. *Applied Geochemistry*, **15**(8): 1071–1083. doi:10.1016/S0883-2927(99)00108-0.

Teo JYQ, Ong A, Tan TTY, et al. 2022. Materials from waste plastics for CO_2 capture and utilisation. *Green Chemistry*, **24**(16): 6086–6099. doi:10.1039/d2gc02306g.

Tester JW, Worley WG, Robinson BA, et al. 1994. Correlating quartz dissolution kinetics in pure water from 25 to 625°C. *Geochimica et Cosmochimica Acta*, **58**(11): 2407–2420. doi:10.1016/0016-7037(94)90020-5.

Tetteh EK, Amankwa MO, Yeboah C, et al. 2021. Emerging carbon abatement technologies to mitigate energy-carbon footprint- a review. *Cleaner Materials*, **2**: 100020. doi:10.1016/j.clema.2021.100020.

Tsakiroglou CD, Terzi K, Aggelopoulos C, et al. 2018. CO_2-induced release of copper and zinc from model soil in water. *International Journal of Greenhouse Gas Control*, **76**: 150–157. doi:10.1016/j.ijggc.2018.07.003.

Um W, Rod KA, Jung HB. 2012. Geochemical alteration of wellbore cement by CO_2 or CO_2+H_2S reaction during long-term carbon storage. *Greenhouse Gases: Science and Technology*, **2**(5): 352–368. doi:10.1002/ghg.

Van Herk J, Pietersen HS, Schuiling RD. 1989. Neutralization of industrial waste acids with olivine - The dissolution of forsteritic olivine at 40-70°C. *Chemical Geology*, **76**(3-4): 341–352. doi:10.1016/0009-2541(89)90102-2.

Vermolen FJ, Gharasoo MG, Zitha PLJ, et al. 2009. Numerical solutions of some diffuse interface problems: The cahn-hilliard equation and the model of Thomas and Windle. *International Journal for Multiscale Computational Engineering*, **7**(6). doi:10.1615/IntJMultCompEng.v7.i6.40.

Voigt M, Marieni C, Baldermann A, et al. 2021. An experimental study of basalt–seawater–CO_2 interaction at 130°C. *Geochimica et Cosmochimica Acta*, **308**: 21–41. doi:10.1016/j.gca.2021.05.056.

Vriens B, Seigneur N, Mayer KU, et al. 2020. Scale dependence of effective geochemical rates in weathering mine waste rock. *Journal of Contaminant Hydrology*. doi:10.1016/j.jconhyd.2020.103699.

Wang H, Wen B, Xu P, et al. 2025. Effect of CO_2 curing on the strength and microstructure of composite waste glass concrete. *Construction and Building Materials*, **463**: 140042. doi:10.1016/j.conbuildmat.2025.140042.

Wang K, Xu T, Tian H, et al. 2016. Impact of mineralogical compositions on different trapping mechanisms during long-term CO_2 storage in deep saline aquifers. *Acta Geotechnica*, **11**(5): 1167–1188. doi:10.1007/s11440-015-0427-3.

Wang X, Pan Y, Fan W, et al. 2025. Fly ash-CaO sorbents prepared via hydration for CO_2 capture in municipal solid waste incineration. *Journal of Environmental Chemical Engineering*, **13**(1): 115103. doi:10.1016/j.jece.2024.115103.

Wang Y, Mao J, Liu X, et al. 2024. Synergistic mechanisms of magnesium slag coupled with dust removal ash for CO_2 sequestration via direct aqueous carbonation: High mineralization efficiency and optimization of reaction parameters. *Construction and Building Materials*, **456**: 138934. doi:10.1016/j.conbuildmat.2024.138934.

Wang Y, Zhang Z, Vuik C, et al. 2023. Simulation of CO_2 Storage Using a Parameterization Method for Essential Trapping Physics: FluidFlower Benchmark Study. *Transport in Porous Media*. doi:10.1007/s11242-023-01987-5.

Waszczuk P, Lutynski M, Gonzalez Gonzalez MA, et al. 2016. Carbon dioxide sorption on EDTA modified halloysite. *E3S Web of Conferences*, **8**: 01054. doi:10.1051/e3sconf/20160801054.

Wells RK, Xiong W, Giammar D, et al. 2017. Dissolution and surface roughening of Columbia River flood basalt at geologic carbon sequestration conditions. *Chemical Geology*, **467**: 100–109. doi:10.1016/j.chemgeo.2017.07.028.

White SK, Spane FA, Schaef HT, et al. 2020. Quantification of CO_2 Mineralization at the Wallula Basalt Pilot Project. *Environmental Science & Technology*, **54**(22): 14609–14616. doi:10.1021/acs.est.0c05142.

Wogelius RA, Walther J. 1991. Olivine dissolution at 25°C: Effects of pH, CO_2, and organic acids. *Geochimica et Cosmochimica Acta*, **55**(4): 943–954. doi:10.1016/0016-7037(91)90153-V.

Wolff-Boenisch D, Gislason SR, Oelkers EH, et al. 2004. The dissolution rates of natural glasses as a function of their composition at pH 4 and 10.6, and temperatures from 25 to 74°C. *Geochimica et Cosmochimica Acta*, **68**(23): 4843–4858. doi:10.1016/j.gca.2004.05.027.

Xia B, Peng J. 2024. Investigating the impact of hot steam on the efficiency of fly ash-CO_2 mineralization: DFT analysis and experimental study. *Journal of Environmental Chemical Engineering*, **12**(3): 114135. doi:10.1016/j.jece.2024.114135.

Xie H, Yue H, Zhu J, et al. 2015. Scientific and engineering progress in CO2 mineralization using industrial waste and natural minerals. *Engineering*, **1**(2): 150–157. doi:10.15302/J-ENG-2015017.

Xie WH, Li H, Yang M, et al. 2022. CO_2 capture and utilization with solid waste. *Green Chemical Engineering*, **3**(3): 199–209. doi:10.1016/j.gce.2022.01.002.

Xiong W, Wells RK, Menefee AH, et al. 2017. CO_2

mineral trapping in fractured basalt. *International Journal of Greenhouse Gas Control*, **66**: 204–217. doi:10.1016/j.ijggc.2017.10.003.

Xu M, Mo L. 2024. Towards sustainable artificial aggregate production using industrial waste and CO_2: A comprehensive review. *Journal of Building Engineering*, **97**: 110823. doi:10.1016/j.jobe.2024.110823.

Xu R, Zhu F, Zou L, et al. 2024. CO_2 mineralization by typical industrial solid wastes for preparing ultrafine $CaCO_3$: A review. *Green Energy & Environment*, **9**(6): 1679–1697. doi:10.1016/j.gee.2024.08.002.

Xu T, Apps JA, Pruess K. 2004. Numerical simulation of CO_2 disposal by mineral trapping in deep aquifers. *Applied Geochemistry*, **19**(7): 917–936. doi:10.1016/j.apgeochem.2003.11.003

Xu T, Sonnenthal E, Spycher N, et al. 2008. TOUGHREACT User's guide: A simulation program for non-isothermal multiphase reactive geochemical transport in variably saturated geologic media, V1.2.1. United States. doi:10.2172/943451.

Yang ZF, Li J, Liang WF, et al. 2016. On the chemical markers of pyroxenite contributions in continental basalts in Eastern China: Implications for source lithology and the origin of basalts. *Earth-Science Reviews*, **157**: 18–31. doi:10.1016/j.earscirev.2016.04.001.

Yao Z, Wang Y, Shen J, et al. 2024. Synergistic CO_2 mineralization using coal fly ash and red mud as a composite system. *International Journal of Coal Science & Technology*, **11**, 37. doi:10.1007/s40789-024-00672-2.

Yekeen N, Padmanabhan E, Sevoo TA, et al. 2020. Wettability of rock/CO_2/brine systems: A critical review of influencing parameters and recent advances. *Journal of Industrial and Engineering Chemistry*, **88**: 1–28. doi:10.1016/j.jiec.2020.03.021.

Yin Y, Zhang L, Deng H, et al. 2024. A perspective on fluid dynamics and geochemistry coupling in geologic CO_2 storage: Key reactions, reactive transport modeling, and upscaling methods. *Gas Science and Engineering*, **130**, 205421. doi:10.1016/j.jgsce.2024.205421.

Yu Z, Yang S, Liu L, et al. 2012. An experimental study on water-rock interaction during water flooding in formations saturated with CO_2. *Acta Petrolei Sinica*, **33**(6): 1032–1042. doi:doi: 10.1016/S0883-2927(99)00048-7

Yuan Q, Zhang J, Zhang S, et al. 2024. An eco-friendly solution for construction and demolition waste: Recycled coarse aggregate with CO_2 utilization. *Science of The Total Environment*, **950**, 175163. doi:10.1016/j.scitotenv.2024.175163.

Zhang ZW, Cui P, Zhu WW. 2022. Deep Learning on Graphs: A Survey. *IEEE Transactions on Knowledge and Data Engineering*. doi:10.1109/TKDE.2020.2981333.

Zhang H, Dong J, Wei C, et al. 2022. Future trend of terminal energy conservation in steelmaking plant: Integration of molten slag heat recovery-combustible gas preparation from waste plastics and CO_2 emission reduction. *Energy*, **239**, 122543. doi:10.1016/j.energy.2021.122543.

Zhang L, Chen L, Hu R, et al. 2022. Subsurface multiphase reactive flow in geologic CO_2 storage: Key impact factors and characterization approaches. *Advances in Geo-Energy Research*, **6**(3): 179–180. doi:10.46690/ager.2022.03.01.

Zhang L, Dzombak DA, Nakles DV, et al. 2013. Characterization of pozzolan-amended wellbore cement exposed to CO_2 and H_2S gas mixtures under geologic carbon storage conditions. *International Journal of Greenhouse Gas Control*, **19**: 358-368. doi:10.1016/j.ijggc.2013.09.004.

Zhang S, Xu Y, Bie X, et al. 2024. Mechanisms in CO_2 gasification and co-gasification of combustible solid waste: A critical review. *Gas Science and Engineering*, **128**, 205368. doi:10.1016/j.jgsce.2024.205368.

Zhang W, Li Y, Xu T, et al. 2009. Long-term variations of CO_2 trapped in different mechanisms in deep saline formations: A case study of the Songliao Basin, China. *International Journal of Greenhouse Gas Control*, **3**(2): 161–180. doi:10.1016/j.ijggc.2008.07.007.

Zhang Z, Pan SY, Li H, et al. 2020. Recent advances in carbon dioxide utilization. *Renewable and Sustainable Energy Reviews*, **125**, 109799. doi:10.1016/j.rser.2020.109799.

Zheng LG, Spycher N, Apps J, et al. 2010. Potential impacts of CO_2 leakage on the quality of fresh water aquifers. In: *13th International Symposium on Water-Rock Interaction (WRI) in mexico, Guanajuato*. CRC Press-Taylor & Francis Group. pp:903–906.